Branched polyethylenes attainable using thermally enhanced bis(imino)acenaphthene-nickel catalysts: exploring the effects of temperature and pressure

Qiuyue Zhang,[a,b] Randi Zhang,[a,b] Yanping Ma,[a,b] Gregory A. Solan,*[a,c] Tongling Liang[a] and Wen-Hua Sun[a,b,d]*

[a] Key Laboratory of Engineering Plastics and Beijing National Laboratory for Molecular Sciences, Institute of Chemistry, Chinese Academy of Sciences, Beijing 100190, China. E-mail. whsun@iccas.ac.cn; Fax: +86-10-62618239; Tel: +86-10-62557955.

[b] CAS Research/Education Center for Excellence in Molecular Sciences and International School, University of Chinese Academy of Sciences, Beijing 100049, China.

[c] Department of Chemistry, University of Leicester, University Road, Leicester LE1 7RH, UK. E-mail: gas8@leicester.ac.uk. Tel.: +44-116-2522096.

[d] State Key Laboratory for Oxo Synthesis and Selective Oxidation, Lanzhou Institute of Chemical Physics, Chinese Academy of Sciences, Lanzhou 730000, China.

Abstract

The 4,4'-difluorobenzhydryl-containing nickel(II) bromide and chloride chelates, [1-[2,6-{(4-F-C_6H_4)$_2$CH}$_2$-4-{C(CH_3)$_3$}-C_6H_2N]-2-(ArN)$C_2C_{10}H_6$]NiX_2 (X = Br: Ar = 2,6-$Me_2C_6H_3$ **Ni1**, 2,6-$Et_2C_6H_3$ **Ni2**, 2,6-*i*-$Pr_2C_6H_3$ **Ni3**, 2,4,6-$Me_3C_6H_2$ **Ni4**, 2,6-Et_2-4-MeC_6H_2 **Ni5**; and X = Cl: Ar = 2,6-$Me_2C_6H_3$ **Ni6**, 2,6-$Et_2C_6H_3$ **Ni7**, 2,6-*i*-$Pr_2C_6H_3$ **Ni8**, 2,4,6-$Me_3C_6H_2$ **Ni9**, 2,6-Et_2-4-MeC_6H_2 **Ni10**), have been prepared and fully characterized. The solid-state structures of representative **Ni3** and **Ni7** display distorted tetrahedral geometries which are maintained in solution with broad paramagnetically shifted resonances a feature of all the ^{1}H and ^{19}F NMR spectra; the effect the halide (Br/Cl) ligand has on the proton and fluorine chemical shifts presents a further point of interest. All ten nickel complexes displayed, on activation with either MAO (methylaluminoxane) or EASC (ethyl aluminum sesquichloride), very high activities (up to 1.36 × 10^7 g PE mol^{-1} (Ni) h^{-1}) for ethylene polymerization at either 1 or 10 atm C_2H_4 with the structural features of the *N,N'*-ligand influential. Significantly, with EASC as co-catalyst, **Ni5** was capable of operating effectively at 90 °C without comprising too much catalytic activity [*ca.* 4.34 × 10^6 g PE mol^{-1} (Ni) h^{-1}]. All the polyethylenes are highly branched with the branching content and type of branch strongly affected by a combination of temperature, pressure and the class of co-catalyst employed. Moreover, good tensile strength (ε_b up to 2839.5%) and elastic recovery (up to 74%) have been displayed, properties that are characteristic of thermoplastic elastomers (TPEs).

Keywords: Nickel catalysts; Branched polyethylene; Temperature and pressure effects; 4,4'-difluorobenzhydryl groups; 1,2-bis(arylimino)acenaphthene

1. Introduction

The discovery of late transition-metal nickel catalysts for ethylene polymerization, particularly those bearing bidentate α-diimine ligands [1,2], has had a major impact on the field of olefin polymerization. Through careful tuning of the steric and electronic properties of the ligand frame and the polymerization conditions, polymers displaying moderately branched through to highly branched structures are accessible [3-10]. In search of more potent nickel catalysts exhibiting improved thermal stability, many studies have focused on modifications to the ligand set. For example, the catalytic performance of α-diimino-nickel precatalysts (**A**, Chart 1) [11] can be improved by using sterically encumbered dibenzhydryl substitution to modify the N-aryl groups in 1,2-bis(arylimino)acenaphthene [12-16], 2-(aryliminomethyl)pyridine [17-22] and 2,3-bis-(arylimino)butane derivatives [23,24,39]; other bulky substituents have also shown potential [6,25,26].

With regard to the unsymmetrical class of bis(imino)acenaphthene (**B**, Chart 1), we have found that modulation of the activity and the structural properties of the polymers can be achieved by changing the *para*-R substituent of the N-2,6-bis(benzhydryl)-phenyl group from methyl [27], to fluoro- [28] through to *tert*-butyl [29]. Notably, t-butyl-containing **B** was not only highly active, but also produced ultra-high molecular weight highly branched polymers ($> 1 \times 10^6$ g mol^{-1}) that showed mechanical properties reminiscent of thermoplastic elastomers (TPEs). However, the moderate thermal stability of this promising catalytic system has limited a more thorough investigation of how physical properties such as temperature influence branching and in turn their mechanical properties. In a separate study, we have found that the introduction of fluorides to the *para*-positions of the N-aryl and benzhydryl groups (**C**, Chart 1) [30,31], can have a positive effect on both the activity and the thermal stability. For example, **C** (R = F, Chart 1), was found to display superior productivity for ethylene polymerization at 70 °C when compared to **B** (R = F) at the same temperature (Chart 1). Elsewhere, computational studies have indicated that the presence of electron withdrawing groups on the N-aryl unit and its substituents can also have a positive effect on the activities of nickel-based catalysts [34-37].

Besides the crucial role played by chelating ligand structure on catalytic activity and polymer branching, physical parameters such as pressure and temperature are undoubtedly also influential. Indeed, such parameters have been explored using zirconium and palladium catalysts for propylene [39,40] and ethylene polymerization [41], respectively. However, only few studies have been undertaken in the context of elastomer formation using nickel-mediated ethylene polymerization.

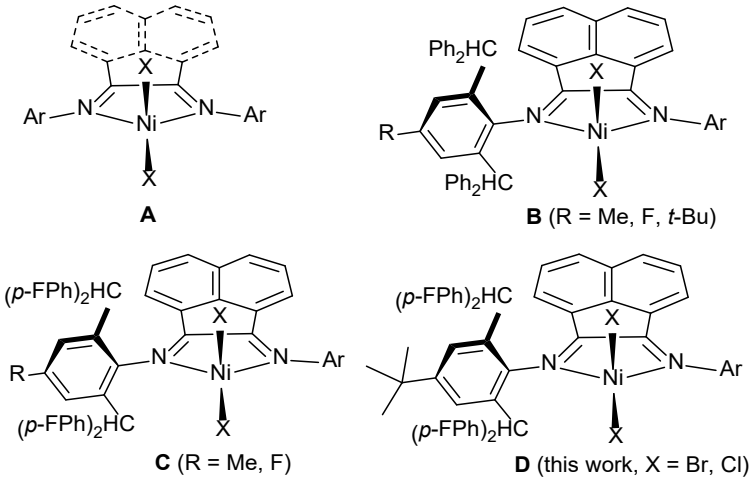

Chart 1 Structural developments in 1,2-bis(imino)acenaphthene-nickel(II) halide precatalysts (**A** – **D**).

Herein, we report a series of unsymmetrical 1,2-bis(arylimino)acenaphthene-nickel(II) halide complexes incorporating one N-2,6-bis(bis(4-fluorophenyl)methyl)-4-*t*-butylphenyl group and one interchangeable aryl group that can be modified in terms of its *ortho*- and *para*-substitution pattern (**D**, Chart 1); the nature of the halide ligand (Br *vs.* Cl) serves as an additional site for variation. An in-depth evaluation of the performance of these 4,4'-difluorobenzhydryl-containing precatalysts for ethylene polymerization is then conducted to explore how the effects of temperature, pressure as well as *N,N′*-ligand type and co-catalyst type impact on both catalytic activity and the branching properties of the polymer. In addition, selected branched samples will be the subject of an investigation of their mechanical properties (*e.g.*, tensile stress-strain and elastic recovery tests) and relevance to TPEs.

2. Experimental

2.1. General considerations

All manipulations involving air and/or moisture sensitive compounds were carried out under an atmosphere of nitrogen using standard Schlenk techniques. Toluene was dried over sodium and distilled under nitrogen atmosphere prior to use. Methylaluminoxane (MAO, 1.46 M in toluene) and modified methylaluminoxane (MMAO, 1.93 M in heptane) were provided by Akzo Nobel Corporation. Diethylaluminum chloride (Et_2AlCl, 1.17 M in toluene) and ethylaluminum sesquichloride ($Et_3Al_2Cl_3$, EASC, 0.87 M in toluene) were purchased from Acros Chemical. High purity ethylene was purchased from Beijing Yanshan Petrochemical Company and used as received. Other reagents were purchased from Aldrich, Acros or local suppliers. The compound 2,6-bis(bis(4-fluorophenyl)methyl)-4-*t*-butylaniline was prepared using a literature route [47]. The ^{1}H and ^{13}C NMR spectra of all organic compounds and nickel complexes were recorded on a Bruker DMX 400 MHz instrument at room temperature using TMS as an internal standard; the ^{19}F NMR spectra were run on a Bruker ADVANCE 600 MHz instrument at ambient temperature were referenced to external CF_3COOH. Elemental analyses were carried out using a Flash EA 1112 microanalyzer. FT-IR spectra were determined on a PerkinElmer System 2000 FT-IR spectrometer. The molecular weight and molecular weight distribution (M_w/M_n) of the polyethylenes were measured using a PL-GPC220 instrument operating at 150 °C with 1,2,4-trichlorobenzene as the solvent. The melting temperatures (T_m) of the polyethylenes were measured from the second scanning run on a PerkinElmer TA-Q2000 DSC analyzer under a nitrogen atmosphere. During this procedure, a sample (4.0 – 6.0 mg) was heated to 150 °C at a rate of 20 °C min^{-1} and kept for 5 min at 150 °C to remove the thermal history and cooled to -20 °C at a rate of 20 °C min^{-1}. For the ^{13}C NMR spectra of the polyethylenes, a weighed amount of polyethylene (80 – 100 mg) was dissolved in 1,1,2,2-tetrachloroethane-d_2 (2 mL) with TMS as an internal standard and inverse gated ^{13}C spectra recorded on a Bruker DMX 300 spectrometer at 75.47 MHz in 5 mm standard glass tubes at 100 °C with the number of scans between 2000 and 3000. Operating conditions used: spectral width 17.9856 kHz; acquisition time 1.8219 s; relaxation delay 2.0 s. An estimation of the branching content was made by integration of the corresponding peaks in the ^{13}C NMR spectra using approaches described in the literature [73]. The stress-strain curves were carried out using a

universal tester (Instron 1122, UK). The stress-strain recovery tests at variable temperatures were conducted by using a dynamic mechanical analyzer (DMA800, TA) under controlled force mode.

2.2. Synthesis of 2-[2,6-bis(bis(4-fluorophenyl)methyl)}-4-t-butylphenylimino]acenaphthylen-1-one

To a suspension of acenaphthylen-1,2-dione (4.0 g, 22.0 mmol) and 2,6-bis(bis(4-fluorophenyl)methyl)-4-*t*-butylaniline (11.0 g, 20.0 mmol) in toluene (100 mL) was added a catalytic amount of *p*-toluenesulfonic acid (0.80 g, 4.0 mmol). The suspension was stirred and heated to reflux for 12 h. On cooling to room temperature, all volatiles were removed under reduced pressure. Dichloromethane (10 mL) was added to dissolve the residue and the solution filtered. Methanol (100 mL) was then added to the filtrate to induce precipitation and this precipitate collected affording 2-[2,6-bis(bis(4-fluorophenyl)methyl)}-4-t-butylphenylimino]acenaphthylen-1-one as orange microcrystals (10.3 g, 72%). FT-IR (cm^{-1}): 3056 (w), 2963 (w), 1896 (w), 1719 ($\nu_{C=O}$, s), 1637 ($\nu_{C=N}$, m), 1595 ($\nu_{C=N}$, m), 1505 (s), 1452 (w), 1360 (w), 1265 (m), 1221 (s), 1184 (w), 1156 (s), 1092 (s), 1014 (m), 907 (m), 874 (w), 835 (m), 780 (m), 731 (w), 687 (w), 661 (m). ^{1}H NMR (400 MHz, CD_2Cl_2, TMS): δ 8.11 (d, *J* = 8.0 Hz, 1H), 8.02 (d, *J* = 8.0 Hz, 1H), 7.86 (d, *J* = 8.4 Hz, 1H), 7.76 (t, *J* = 7.6 Hz, 1H), 7.12 (t, *J* = 7.8 Hz, 1H), 7.00-6.94 (m, 10H), 6.82-6.75 (m, 4H), 6.39-6.34 (m, 4H), 6.11 (d, *J* = 7.2 Hz, 1H), 5.35 (s, 2H), 1.14(s, 9H). ^{13}C NMR (75 MHz, CD_2Cl_2): δ 188.7, 162.3, 161.9, 161.7, 159.9, 159.2, 146.8, 145.4, 142.0, 138.4, 137.5, 131.7, 130.7, 130.4, 130.3, 130.0, 129.8, 128.7, 128.1, 127.6, 127.0, 126.6, 124.7, 123.0, 121.2, 115.0, 114.8, 114.6, 114.4, 114.2, 50.4, 33.9, 30.7.

2.3. Synthesis of L1 – L5

2.3.1. 1-[2,6-{(4-F-C_6H_4)$_2$CH}$_2$-4-{C(CH_3)$_3$}-C_6H_2N]-2-(2,6-$Me_2C_6H_3N$)$C_2C_{10}H_6$ (**L1**)

A round bottom flask, equipped with condenser and stir bar, was loaded with 2-[2,6-bis(bis(4-fluorophenyl)methyl)}-4-t-butylphenylimino]acenaphthylen-1-one (1.44 g, 2.00 mmol), a catalytic amount of *para*-toluenesulfonic acid (0.08 g, 0.40 mmol) and toluene (20 mL) and the contents stirred and heated to reflux until complete dissolution was observed.

2,6-Dimethylaniline (0.36 g, 3.00 mmol) was then added dropwise to the solution and the reaction mixture maintained at reflux for a further 12 h. On completion of the reaction, the mixture was cooled to room temperature and the volatiles evaporated under reduced pressure. The crude product was purified by basic alumina column chromatography with petroleum ether/ethyl acetate (v/v = 50:1) as the eluent to afford **L1** as an orange powder (0.53 g, 32%). FT-IR (cm^{-1}): 2960 (w), 2362 (w), 1663 ($\nu_{C=N}$, m), 1641 ($\nu_{C=N}$, w), 1598 (m), 1504 (s), 1468 (m), 1442 (m), 1361 (w), 1255 (w), 1220 (s), 1155 (m), 1092 (m), 1037 (w), 1014 (m), 922 (m), 877 (w), 828 (s), 781 (m), 726 (w), 658 (w). Anal. Calcd for $C_{56}H_{44}F_4N_2$ (820.98): H, 5.40; N, 3.41; C, 81.93. Found: H, 5.77; N, 3.38; C, 81.77%. ^{1}H NMR (400 MHz, CD_2Cl_2, TMS): δ 7.83 (d, *J* = 8.4 Hz, 1H), 7.78 (d, *J* = 8 Hz, 1H), 7.31 (t, *J* = 7.6 Hz, 1H), 7.18-6.93 (m, 14H), 6.83 (t, *J* = 7.0 Hz, 4H), 6.57 (d, *J* = 7.2 Hz, 1H), 6.40 (t, *J* = 8.6 Hz, 4H), 6.19 (d, *J* = 6.8 Hz, 1H), 5.51 (s, 2H), 2.12 (s, 6H), 1.17 (s, 9H). ^{13}C NMR (100 MHz, CD_2Cl_2): δ 162.5, 162.2, 161.5, 160.4, 159.7, 159.1, 148.8, 146.0, 145.9, 139.4, 138.5, 138.4, 137.6, 130.7, 130.6, 130.4, 130.3, 129.9, 128.4, 128.2, 127.9, 127.4, 126.6, 124.6, 124.1, 123.2, 122.9, 121.6, 114.5, 114.2, 114.0, 50.4, 33.9, 30.6, 17.4. ^{19}F NMR (470 MHz, $CDCl_3$): δ -117.1, -117.3.

2.3.2. 1-[2,6-{(4-F-C_6H_4)$_2$CH}$_2$-4-{$C(CH_3)_3$}-C_6H_2N]-2-(2,6-$Et_2C_6H_3N$)$C_2C_{10}H_6$ (**L2**)

Using the same procedure and molar ratios of reactants as that outlined for the synthesis of **L1** but with 2,6-diethylaniline as the amine, **L2** was isolated an orange solid (0.61 g, 37%). FT-IR (cm^{-1}): 2966 (w), 2872 (w), 2362 (w), 1666 ($\nu_{C=N}$, m), 1641 ($\nu_{C=N}$, w), 1598 (m), 1505 (s), 1449 (m), 1364 (w), 1259 (w), 1221 (s), 1155 (m), 1096 (m), 1016 (w), 924 (m), 875 (w), 827 (s), 800 (m), 778 (m), 757 (m), 728 (m), 699 (w). Anal. Calcd for $C_{58}H_{48}F_4N_2$ (849.03): H, 5.70; N, 3.30; C, 82.05. Found: H, 5.69; N, 3.30; C, 81.86%. ^{1}H NMR (400 MHz, CD_2Cl_2, TMS): δ 7.78 (d, *J* = 8.8 Hz, 1H), 7.74 (d, *J* = 8.0 Hz, 1H), 7.25 (t, *J* = 15.2 Hz, 1H), 7.22-7.04 (m, 3H), 7.01 (t, *J* = 4.0 Hz, 1H), 6.97-6.93 (m, 10H), 6.82 (m, 4H), 6.53 (d, *J* = 7.2 Hz, 1H), 6.39 (t, *J* = 5.7 Hz, 4H), 6.12 (d, *J* = 8.6 Hz, 1H), 5.51 (s, 2H), 2.57-2.53 (m, 2H), 2.43-2.40 (m, 2H), 1.17 (s, 9H), 1.15 (t, *J* = 8.0 Hz, 6H). ^{13}C NMR (100 MHz, CD_2Cl_2): δ 161.6, 160.6, 160.0, 159.2, 149.0, 146.1, 146.0, 139.6, 138.7, 137.7, 130.8, 130.7, 130.5, 130.4, 130.1, 130.0, 128.5, 128.3, 127.3, 126.7, 126.0, 124.8, 123.8, 123.2, 122.3, 114.6, 114.4, 114.1, 50.5, 34.1, 30.8, 24.2, 13.8. ^{19}F NMR (470 MHz, $CDCl_3$): δ -117.1, -117.2.

2.3.3. 1-[2,6-{(4-F-C_6H_4)$_2$CH}$_2$-4-{C(CH_3)$_3$}-C_6H_2N]-2-(2,6-*i*-$Pr_2C_6H_3$N)$C_2C_{10}H_6$ (**L3**)

Using the same procedure and molar ratios of reactants as that outlined for the synthesis of **L1** but with 2,6-diisopropylaniline as the amine, **L3** was isolated as an orange solid (0.46 g, 26%). FT-IR (cm^{-1}): 2961 (m), 2869 (w), 1663 ($\nu_{C=N}$, m), 1640 ($\nu_{C=N}$, w), 1597 (m), 1505 (s), 1463 (m), 1361 (w), 1324 (w), 1224 (s), 1157 (m), 1096 (m), 1040 (w), 1015 (w), 923 (m), 875 (w), 830 (s), 781 (m), 756 (m), 729 (m), 662 (w). Anal. Calcd for $C_{60}H_{52}F_4N_2$ (877.08): H, 5.98; N, 3.19; C, 82.17. Found: H, 6.20; N, 3.13; C, 81.85%. ^{1}H NMR (400 MHz, CD_2Cl_2, TMS): δ 7.80 (d, *J* = 8.0 Hz, 1H), 7.74 (d, *J* = 8.0 Hz, 1H), 7.28-7.22 (m, 5H), 7.09-6.94 (m, 10H), 6.82 (t, *J* = 6.0 Hz, 4H), 6.49 (d, *J* = 7.1 Hz, 1H), 6.38 (t, *J* = 7.8 Hz, 4H), 6.10 (d, *J* = 6.8 Hz, 1H), 5.51 (s, 2H), 2.98-2.95 (m, 2H), 1.23 (d, *J* = 6.4 Hz, 6H), 1.55 (s, 9H), 0.99 (d, *J* = 6.8 Hz, 6H). ^{13}C NMR (100 MHz, CD_2Cl_2): δ 162.7, 162.3, 161.6, 161.0, 159.8, 159.1, 146.6, 146.1, 146.0, 139.7, 138.6, 137.7, 134.8, 130.7, 130.6, 130.4, 130.4, 129.9, 128.5, 128.3, 128.2, 128.1, 127.0, 126.6, 124.8, 124.1, 123.2, 123.1, 122.7, 114.5, 114.3, 114.1, 50.4, 34.0, 30.7, 28.0, 23.0, 22.9. ^{19}F NMR (470 MHz, $CDCl_3$): δ -117.1, -117.2.

2.3.4. 1-[2,6-{(4-F-C_6H_4)$_2$CH}$_2$-4-{C(CH_3)$_3$}-C_6H_2N]-2-(2,4,6-$Me_3C_6H_2$N)$C_2C_{10}H_6$ (**L4**)

Using the same procedure and molar ratios of reactants as that outlined for the synthesis of **L1** but with 2,4,6-trimethylaniline as the amine, **L4** was isolated as an orange solid (0.41 g, 24%). FT-IR (cm^{-1}): 2963 (w), 1668 ($\nu_{C=N}$, m), 1642 ($\nu_{C=N}$, w), 1599 (m), 1505 (s), 1449 (m), 1364 (w), 1258 (w), 1221 (s), 1155 (m), 1095 (m), 1041 (w), 1015 (w), 923 (m), 876 (w), 828 (s), 798 (w), 780 (m), 757 (w), 727 (m), 699 (w), 660 (w). Anal. Calcd for $C_{57}H_{46}F_4N_2$ (835.00): H, 5.55; N, 3.35; C, 81.99. Found: H, 5.56; N, 3.33; C, 81.69%. ^{1}H NMR (400 MHz, CD_2Cl_2, TMS): δ 7.82 (d, *J* = 8.4 Hz, 1H), 7.77 (d, *J* = 8.0 Hz, 1H), 7.32 (t, *J* = 7.0 Hz, 1H), 7.10-6.94 (m, 13H), 6.83 (t, *J* = 6.2 Hz, 4H), 6.63 (d, *J* = 7.2 Hz, 1H), 6.40 (t, *J* = 8.0 Hz, 4H), 6.19 (d, *J* = 3.4 Hz, 1H), 5.50 (s, 2H), 2.37 (s, 3H), 2.08 (s, 6H), 1.17 (s, 9H). ^{13}C NMR (100 MHz CD_2Cl_2): δ 161.6, 160.7, 159.8, 159.2, 146.3, 146.0, 139.5, 138.6, 138.5, 138.2, 137.7, 130.8, 130.7, 130.5, 130.4, 130.0, 128.6, 128.4, 128.3, 127.4, 126.6, 125.0, 124.6, 123.9, 122.9, 121.7, 114.9, 114.7, 114.5, 114.3, 114.2, 114.0, 50.5, 34.0, 30.7, 20.2, 17.4. ^{19}F NMR (470 MHz, $CDCl_3$): δ -117.1, -117.3.

2.3.5. 1-[2,6-{(4-F-C_6H_4)$_2$CH}$_2$-4-{C(CH_3)$_3$}-C_6H_2N]-2-(2,6-Et_2-4-MeC_6H_2N)$C_2C_{10}H_6$ (**L5**)

Using the same procedure and molar ratios of reactants as that outlined for the synthesis of **L1** but with 2,6-diethyl-4-methylaniline as the amine, **L5** was isolated as an orange solid (0.46 g, 27%). FT-IR (cm^{-1}): 2962 (w), 1666 ($\nu_{C=N}$, m), 1642 ($\nu_{C=N}$, w), 1599 (m), 1505 (s), 1452 (m), 1362 (w), 1258 (w), 1214 (s), 1155 (m), 1094 (m), 1037 (w), 1016 (w), 916 (m), 879 (w), 829 (s), 779 (m), 726 (m), 660 (w). Anal. Calcd for $C_{59}H_{50}F_4N_2$ (863.06): H, 5.84; N, 3.25; C, 82.11. Found: H, 5.91; N, 3.23; C, 81.86%. ^{1}H NMR (400 MHz, CD_2Cl_2, TMS): δ 7.81 (d, *J* = 8.0 Hz, 1H), 7.75 (d, *J* = 8.4 Hz, 1H), 7.30 (t, *J* = 7.6 Hz, 1H), 7.10-6.93 (m, 13H), 6.83 (t, *J* = 6.6 Hz, 4H), 6.61 (d, *J* = 7.2 Hz, 1H), 6.39 (t, *J* = 8.4 Hz, 4H), 6.12 (d, *J* = 7.2 Hz, 1H), 5.51 (s, 2H), 2.57-2.47 (m, 2H), 2.41-2.3 (m, 5H), 1.18 (s, 9H), 1.11 (t, *J* = 7.6 Hz, 6H). ^{13}C NMR (100 MHz, CD_2Cl_2): δ 162.3, 161.6, 160.9, 159.9, 159.2, 146.1, 145.4, 139.6, 138.7, 137.7, 133.1, 130.8, 130.7, 130.5, 130.4, 129.9, 128.6, 128.4, 128.2, 127.3, 126.8, 126.6, 124.8, 123.1, 122.3, 114.5, 114.2, 114.1, 50.4, 34.0, 30.7, 24.2, 20.5, 13.9. ^{19}F NMR (470 MHz, $CDCl_3$): δ -117.1, -117.3.

2.4. Synthesis of Ni1 – Ni5

2.4.1. [1-[2,6-{(4-F-C_6H_4)$_2$CH}$_2$-4-{C(CH_3)$_3$}-C_6H_2N]-2-(2,6-$Me_2C_6H_3$N)$C_2C_{10}H_6$]$NiBr_2$ (**Ni1**)

Under an atmosphere of nitrogen, dichloromethane (10 mL) was added to a mixture of **L1** (0.082 g, 0.10 mmol) and (DME)$NiBr_2$ (0.031 g, 0.10 mmol). After stirring for 12 h at room temperature, the mixture become yellow in color. The solvent was concentrated to *ca.* 3 mL and diethyl ether (20 mL) added to induce precipitation. The solid was collected by filtration and washed with diethyl ether to form **Ni1** as a deep red solid (0.083 g, 80%). FT-IR (cm^{-1}): 2955 (w), 1651 ($\nu_{C=N}$, w), 1626 ($\nu_{C=N}$, m), 1602 (m), 1506 (s), 1295 (w), 1219 (s), 1158 (s), 1117 (w), 1047 (w), 1015 (w), 878 (w), 833 (s), 776 (m), 729 (w). Anal. Calcd for $C_{56}H_{44}Br_2F_4N_2Ni$ (1039.48): H, 4.27; N, 2.70; C, 64.71. Found: H, 4.52; N, 2.64; C, 64.36%. ^{1}H NMR (400 MHz, $CDCl_3$, TMS): δ 28.96 (s, 6H, –CH_3), 25.47 (s, 2H, Ar–Hm), 24.96 (s, 1H, An–H), 22.74 (s, 2H, Ar–Hm), 20.43 (s, 1H, An–H), 17.27 (s, 1H, An–H), 16.46 (s, 1H, An–H), 12.95 (broad, 1.2H, –$CHPh_2F_2$), 8.03 (s, 5H, Ar–H), 7.01 (s, 6H, Ar–H), 5.99 (s, 1H, An–H), 5.47 (s, 5H, Ar–H), 4.96 (s, 1H, An–H), 3.56 (s, 9H, −C(CH_3)$_3$), −15.73 (s, 1H, Ar–Hp). ^{19}F NMR (470 MHz, $CDCl_3$): δ -116.6, -117.1.

2.4.2. [1-[2,6-{(4-F-C_6H_4)$_2$CH}$_2$-4-{C(CH_3)$_3$}-C_6H_2N]-2-(2,6-$Et_2C_6H_3$N)$C_2C_{10}H_6$]$NiBr_2$ (**Ni2**)

Using the same procedure and molar ratios of reactants as that outlined for the synthesis of **Ni1** but with **L2** as the 1,2-bis(imino)acenaphthene, **Ni2** was isolated as a deep red solid (0.090 g, 84%). FT-IR (cm^{-1}): 2967 (m), 2971 (w), 1650 ($\nu_{C=N}$, m), 1621 ($\nu_{C=N}$, w), 1604 (m), 1506 (s), 1416 (m), 1373 (w), 1294 (w), 1224 (s), 1157 (s), 1110 (m), 1043 (w), 1017 (w), 934 (w), 877 (w), 837 (s), 779 (m), 732 (w). Anal. Calcd for $C_{58}H_{48}Br_2F_4N_2Ni$ (1067.53): H, 4.53; N, 2.62; C, 65.26. Found: H, 4.68; N, 2.55; C, 65.16%. ^{1}H NMR (400 MHz, $CDCl_3$, TMS): δ 28.02 (s, 2H, –CH_2CH_3), 27.90 (s, 2H, –CH_2CH_3), 26.84 (s, 2H, Ar–Hm), 25.34 (s, 1H, An–H), 22.89 (s, 2H, Ar–Hm), 20.53 (s, 1H, An–H), 17.22 (s, 1H, An–H), 16.49 (s, 1H, An–H), 12.95 (broad, 1.1H, –$CHPh_2F_2$), 8.01 (s, 5H, Ar–H), 6.97 (s, 6H, Ar–H), 5.93 (s, 1H, An–H), 5.48 (s, 5H, Ar–H), 4.93 (s, 1H, An–H), 3.57 (s, 9H, −C(CH_3)$_3$), 0.61 (s, 6H, −CH_2CH_3), −16.50 (s, 1H, Ar–Hp). ^{19}F NMR (470 MHz, $CDCl_3$): δ -116.6, -117.1.

2.4.3. [1-[2,6-{(4-F-C_6H_4)$_2$CH}$_2$-4-{C(CH_3)$_3$}-C_6H_2N]-2-(2,6-*i*-$Pr_2C_6H_3$N)$C_2C_{10}H_6$]$NiBr_2$ (**Ni3**)

Using the same procedure and molar ratios of reactants as that outlined for the synthesis of **Ni1** but with **L3** as the 1,2-bis(imino)acenaphthene, **Ni3** was isolated as a deep red solid (0.088 g, 80%). FT-IR (cm^{-1}): 2968 (m), 2867 (w), 1647 ($\nu_{C=N}$, m), 1622 ($\nu_{C=N}$, m), 1601 (m), 1583 (w), 1505 (s), 1465 (w), 1421 (m), 1363 (w), 1293 (w), 1222 (s), 1189 (w), 1158 (s), 1114 (m), 1047 (w), 1015 (w), 933 (w), 877 (w), 833 (s), 803 (m), 778 (w). Anal. Calcd for $C_{60}H_{52}Br_2F_4N_2Ni$ (1095.59): H, 4.78; N, 2.56; C, 65.78. Found: H, 4.97; N, 2.49; C, 65.96%. ^{1}H NMR (400 MHz, $CDCl_3$, TMS): δ 25.54 (s, 1H, An–H), 24.95 (s, 2H, Ar–Hm), 23.33 (s, 2H, Ar–Hm), 17.71 (s, 1H, An–H), 17.69 (s, 1H, An–H), 16.66 (s, 1H, An–H), 13.64 (broad, 1.2H, –$CHPh_2F_2$), 7.94 (s, 5H, Ar–H), 6.92 (s, 6H, Ar–H), 5.64 (s, 6H, 6 × Ar–*H*, An–*H*), 5.04 (s, 1H, An–H), 3.65 (s, 9H, −C(CH_3)$_3$), 1.64 (s, 12H, −CH(CH_3)$_2$), 1.44 (s, 2H, −CH(CH_3)$_2$), −16.22 (s, 1H, Ar–Hp). ^{19}F NMR (470 MHz, $CDCl_3$): δ -116.5, -117.2.

2.4.4. [1-[2,6-{(4-F-C_6H_4)$_2$CH}$_2$-4-{C(CH_3)$_3$}-C_6H_2N]-2-(2,4,6-$Me_3C_6H_2$N)$C_2C_{10}H_6$]$NiBr_2$ (**Ni4**)

Using the same procedure and molar ratios of reactants as that outlined for the synthesis of **Ni1** but with **L4** as the 1,2-bis(imino)acenaphthene, **Ni4** was isolated as a deep red solid (0.088 g, 83%). FT-IR (cm^{-1}): 2965 (m), 1647 ($\nu_{C=N}$, m), 1623 ($\nu_{C=N}$, m), 1601 (m), 1506 (s), 1451 (w), 1294 (w), 1223 (s), 1191 (w), 1158 (s), 1097 (m), 1049 (w), 1016 (w), 932 (w), 877 (w), 834 (s), 805 (m), 776 (m). Anal. Calcd for $C_{57}H_{46}Br_2F_4N_2Ni$ (1053.50): H, 4.40; N, 2.66; C, 64.99. Found: H, 4.62; N, 2.60; C, 64.79%. ^{1}H NMR (400 MHz, $CDCl_3$, TMS): δ 34.49 (s, 3H, Ar–p–CH_3), 29.18 (s, 6H, –CH_3), 25.54 (s, 1H, An–H), 25.32 (s, 2H, Ar–Hm), 22.77 (s, 2H, Ar–Hm), 20.28 (s, 1H, An–H), 17.25 (s, 1H, An–H), 16.50 (s, 1H, An–H), 12.78 (broad, 1.2H, –$CHPh_2F_2$), 8.08 (s, 5H, Ar–H), 7.02 (s, 6H, Ar–H), 6.04 (s, 1H, An–H), 5.44 (s, 5H, Ar–H), 4.87 (s, 1H, An–H), 3.52 (s, 9H, −$C(CH_3)_3$). ^{19}F NMR (470 MHz, $CDCl_3$): δ -116.7, -117.1.

2.4.5. [1-[2,6-{(4-F-C_6H_4)$_2$CH}$_2$-4-{$C(CH_3)_3$}-C_6H_2N]-2-(2,6-Et_2-4-MeC_6H_2N)$C_2C_{10}H_6$]$NiBr_2$ (**Ni5**)

Using the same procedure and molar ratios of reactants as that outlined for the synthesis of **Ni1** but with **L5** as the 1,2-bis(imino)acenaphthene, **Ni5** was isolated as a deep red solid (0.088 g, 81%). FT-IR (cm^{-1}): 2965 (m), 1650 ($\nu_{C=N}$, m), 1626 ($\nu_{C=N}$, m), 1602 (m), 1506 (s), 1295 (m), 1267 (w), 1218 (s), 1194 (w), 1158 (s), 1117 (m), 1047 (w), 1015 (w), 878 (w), 833 (s), 775 (m). Anal. Calcd For $C_{59}H_{50}Br_2F_4N_2Ni$ (1081.56): H, 4.66; N, 2.59; C, 65.52. Found: H, 4.80; N, 2.52; C, 65.42%. ^{1}H NMR (400 MHz, $CDCl_3$, TMS): δ 34.50 (s, 3H, Ar–p–CH_3), 27.78 (s, 2H, –CH_2CH_3), 27.09 (s, 2H, –CH_2CH_3), 25.70 (s, 1H, An–H), 25.06 (s, 2H, Ar–Hm), 22.88 (s, 2H, Ar–Hm), 20.36 (s, 1H, An–H), 17.20 (s, 1H, An–H), 16.53 (s, 1H, An–H), 12.86 (broad, 1.2H, –$CHPh_2F_2$), 8.00 (s, 5H, Ar–H), 6.99 (s, 6H, Ar–H), 6.00 (s, 1H, An–H), 5.49 (s, 5H, Ar–H), 4.89 (s, 1H, An–H), 3.54 (s, 9H, −$C(CH_3)_3$), 0.61 (s, 6H, −CH_2CH_3). ^{19}F NMR (470 MHz, $CDCl_3$): δ -116.6, -117.1.

2.5. Synthesis of Ni6 – Ni10

2.5.1. [1-[2,6-{(4-F-C_6H_4)$_2$CH}$_2$-4-{$C(CH_3)_3$}-C_6H_2N]-2-(2,6-$Me_2C_6H_3$N)$C_2C_{10}H_6$]$NiCl_2$ (**Ni6**)

Under an atmosphere of nitrogen, a mixed solvent system composed of dichloromethane and ethanol (5/5 mL) was added to a flask containing **L1** (0.083 g, 0.10 mmol) and $NiCl_2{\cdot}6H_2O$ (0.023 g, 0.10 mmol). After stirring for 24 h at ambient temperature, the solvent was concentrated to *ca.* 3

mL and diethyl ether (20 mL) added to induce precipitation. The solid was collected by filtration and washed with diethyl ether to afford **Ni6** as a light orange powder (0.073 g, 77%). FT-IR (cm^{-1}): 2955 (m), 1645 ($\nu_{C=N}$, m), 1630 ($\nu_{C=N}$, m), 1600 (m), 1505 (s), 1293 (m), 1220 (s), 1194 (w), 1158 (s), 1115 (m), 1044 (w), 1014 (w), 936 (w), 878 (w), 833 (s), 774 (m). Anal. Calcd for $C_{56}H_{44}Cl_2F_4N_2Ni$ (950.57): H, 4.67; N, 2.95; C, 70.76. Found: H, 5.02; N, 2.90; C, 70.56%. ^{1}H NMR (400 MHz, $CDCl_3$, TMS): δ 27.10 (s, 9H, 2×C*H*$_3$, An–*H*, 2×Ar–*H*m), 24.00 (s, 2H, Ar–Hm), 20.95 (s, 1H, An–H), 16.83 (s, 1H, An–H), 16.09 (s, 1H, An–H), 11.76 (broad, 0.7H, –CHPh$_2$F$_2$), 7.94 (s, 5H, Ar–H), 6.80 (s, 6H, Ar–H), 5.91 (s, 1H, An–H), 5.30 (s, 5H, Ar–H), 4.03 (s, 10H, An–*H*, C(C*H*$_3$)$_3$), -15.25 (s, 1H, Ar–Hp). ^{19}F NMR (470 MHz, $CDCl_3$): δ -117.1, -117.2, -117.4.

2.5.2. [1-[2,6-{(4-F-C_6H_4)$_2$CH}$_2$-4-{C(CH_3)$_3$}-C_6H_2N]-2-(2,6-$Et_2C_6H_3$N)$C_2C_{10}H_6$]$NiCl_2$ (**Ni7**)

Using the same procedure and molar ratios of reactants as that outlined for the synthesis of **Ni6** but with **L2** as the 1,2-bis(imino)acenaphthene, **Ni7** was isolated as a deep orange solid (0.078 g, 80%). FT-IR (cm^{-1}): 2966 (m), 1651 ($\nu_{C=N}$, m), 1625 ($\nu_{C=N}$, m), 1602 (m), 1508 (s), 1450 (w), 1423 (w), 1295 (m), 1227 (s), 1190 (w), 1159 (s), 1098 (m), 1052 (w), 838 (s), 776 (m). Anal. Calcd for $C_{58}H_{48}Cl_2F_4N_2Ni$ (978.62): H, 4.94; N, 2.86; C, 71.19. Found: H, 5.18; N, 2.83; C, 71.56%. ^{1}H NMR (400 MHz, $CDCl_3$, TMS): δ 25.60 (s, 2H, Ar–Hm), 25.54 (s, 2H, –CH_2CH_3), 24.92 (s, 1H, An–H), 24.50 (s, 2H, Ar–Hm), 23.56 (s, 2H, –CH_2CH_3), 21.52 (s, 1H, An–H), 17.06 (s, 1H, An–H), 16.41 (s, 1H, An–H), 12.95 (broad, 1.4H, –CHPh$_2$F$_2$), 8.08 (s, 5H, Ar–H), 6.91 (s, 6H, Ar–H), 5.75 (s, 1H, An–H), 5.15 (s, 5H, Ar–H), 4.32 (s, 10H, An–*H*, C(C*H*$_3$)$_3$), 0.32 (s, 6H, −CH_2CH_3), −15.04 (s, 1H, Ar–Hp). ^{19}F NMR (470 MHz, $CDCl_3$) δ -117.1, -117.2, -117.4.

2.5.3. [1-[2,6-{(4-F-C_6H_4)$_2$CH}$_2$-4-{C(CH_3)$_3$}-C_6H_2N]-2-(2,6-*i*-$Pr_2C_6H_3$N)$C_2C_{10}H_6$]$NiCl_2$ (**Ni8**)

Using the same procedure and molar ratios of reactants as that outlined for the synthesis of **Ni6** but with **L3** as the 1,2-bis(imino)acenaphthene, **Ni8** was isolated as a light orange solid (0.088 g, 87%). FT-IR (cm^{-1}): 2966 (m), 1649 ($\nu_{C=N}$, m), 1622 ($\nu_{C=N}$, m), 1601 (m), 1506 (s), 1467 (m), 1363 (w), 1292 (w), 1224 (s), 1189 (w), 1158 (s), 1115 (m), 1048 (w), 1016 (w), 935 (w), 877 (w), 835 (s), 804 (m), 778 (m). Anal. Calcd for $C_{60}H_{52}Cl_2F_4N_2Ni$ (1006.68): H, 5.21; N, 2.78; C, 71.59. Found: H, 5.37; N, 2.71; C, 71.36%. ^{1}H NMR (400 MHz, $CDCl_3$, TMS): δ 26.29 (s, 2H, Ar–Hm), 25.65 (s,

1H, An–H), 25.12 (s, 2H, Ar–Hm), 22.21 (s, 1H, An–H), 17.55 (s, 1H, An–H), 16.60 (s, 1H, An–H), 12.48 (broad, 1.7H, –$CHPh_2F_2$), 7.97 (s, 5H, Ar–H), 6.80 (s, 6H, Ar–H), 5.43 (s, 1H, An–H), 5.17 (s, 5H, Ar–H), 5.14 (s, 1H, An–H), 4.47 (s, 9H, −$C(CH_3)_3$), 3.44 (s, 2H, −$CH(CH_3)_2$), 1.20 (s, 12H, −$CH(CH_3)_2$), −14.75 (s, 1H, Ar–Hp). ^{19}F NMR (470 MHz, $CDCl_3$): δ -117.1, -117.2, -117.3.

2.5.4. [1-[2,6-{(4-F-C_6H_4)$_2$CH}$_2$-4-{$C(CH_3)_3$}-C_6H_2N]-2-(2,4,6-$Me_3C_6H_2N$)$C_2C_{10}H_6$]$NiCl_2$ (**Ni9**)

Using the same procedure and molar ratios of reactants as that outlined for the synthesis of **Ni6** but with **L4** as the 1,2-bis(imino)acenaphthene, **Ni9** was isolated as a deep orange solid (0.068 g, 70%). FT-IR (cm^{-1}): 2954 (m), 1651 ($\nu_{C=N}$, m), 1630 ($\nu_{C=N}$, m), 1602 (m), 1506 (s), 1477 (w), 1293 (m), 1225 (s), 1194 (w), 1158 (s), 1098 (w), 1044 (w), 1016 (w), 934 (w), 836 (s), 776 (m). Anal. Calcd for $C_{57}H_{46}Cl_2F_4N_2Ni$ (964.60): H, 4.81; N, 2.90; C, 70.98. Found: H, 5.02; N, 2.82; C, 70.69%. ^{1}H NMR (400 MHz, $CDCl_3$, TMS): δ 35.05 (s, 3H, Ar–p–CH_3), 27.38 (s, 9H, 2 × C*H*$_3$, An–*H*, 2 × Ar–*H*m), 24.08 (s, 2H, Ar–Hm), 21.25 (s, 1H, An–H), 16.90 (s, 1H, An–H), 16.13 (s, 1H, An–H), 11.28 (broad, 1.2H, –$CHPh_2F_2$), 8.01 (s, 5H, Ar–H), 6.83 (s, 6H, Ar–H), 5.94 (s, 1H, An–H), 5.25 (s, 5H, Ar–H), 4.03 (s, 10H, An–*H*, C(C*H*$_3$)$_3$). ^{19}F NMR (470 MHz, $CDCl_3$): δ -117.1, -117.2, -117.4.

2.5.5. [1-[2,6-{(4-F-C_6H_4)$_2$CH}$_2$-4-{$C(CH_3)_3$}-C_6H_2N]-2-(2,6-Et_2-4-MeC_6H_2N)$C_2C_{10}H_6$]$NiCl_2$ (**Ni10**)

Using the same procedure and molar ratios of reactants as that outlined for the synthesis of **Ni6** but with **L5** as the 1,2-bis(imino)acenaphthene, **Ni10** was isolated as a dark yellow powder (0.075 g, 75%). FT-IR (cm^{-1}): 2962 (m), 1650 ($\nu_{C=N}$, m), 1630 ($\nu_{C=N}$, m), 1600 (m), 1505 (s), 1458 (w), 1291 (m), 1223 (s), 1186 (w), 1158 (s), 1096 (w), 1047 (w), 1017 (w), 928 (w), 836 (s), 777 (m). Anal. Calcd for $C_{59}H_{50}Cl_2F_4N_2Ni$ (992.65): H, 5.08; N, 2. 82; C, 71.39. Found: H, 5.26; N, 2.76; C, 71.65%. ^{1}H NMR (400 MHz, $CDCl_3$, TMS): δ 34.88 (s, 3H, Ar–p–CH_3), 26.07 (s, 2H, –CH_2CH_3), 25.46 (s, 3H, –C*H*$_2$CH$_3$, An–*H*), 24.44 ((s, 2H, Ar–Hm), 23.82 (s, 2H, Ar–Hm), 21.36 (s, 1H, An–H), 17.05 (s, 1H, An–H), 16.45 (s, 1H, An–H), 11.86 (broad, 1.5H, –$CHPh_2F_2$), 8.12 (s, 5H,

Ar–H), 6.89 (s, 6H, Ar–H), 6.29 (s, 1H, An–H), 5.81 (s, 1H, An–H), 5.60 (s, 5H, Ar–H), 4.32 (s, 9H, −C(CH_3)$_3$), 0.36 (s, 6H, −CH_2CH_3). ^{19}F NMR (470 MHz, $CDCl_3$): δ -117.1, -117.2, -117.4.

2.6. X-ray crystallographic studies

Single crystals of **Ni3** and **Ni7** were obtained by layering diethyl ether onto their dichloromethane solutions at ambient temperature. X-ray determinations were carried out on a Rigaku Saturn 724+ CCD with graphite-monochromatic Mo-Kα radiation (λ = 0.71073 Å) at 173(2) K and the cell parameters obtained by global refinement of the positions of all collected reflections. Intensities were corrected for Lorentz and polarization effects and empirical absorption. Details of data collection, refinement and crystal data are listed in Table S9. Structure solution by direct methods and structure refinement based on full-matrix least-squares on F^2 employed SHELXT (Sheldrick, 2015) [71,72]. All hydrogen atoms were placed in calculated positions and all non-hydrogen atoms refined anisotropically.

2.7. Typical procedures for ethylene polymerization

2.7.1. Ethylene polymerization at 1 atm C_2H_4.

The polymerization at 1 atm C_2H_4 was performed in a 50 mL oven-dried Schlenk flask. Under an ethylene atmosphere (1 atm), the precatalyst (2.0 μmol) was added followed by freshly distilled toluene (30 mL) and the required amount of co-catalyst (*i.e.*, MAO or EASC) then introduced by syringe. The solution was then stirred at room temperature under an ethylene atmosphere (1 atm). After 30 min, the pressure was vented and the solution quenched with 10% hydrochloric acid in ethanol. The polymer was collected by filtration and washed with ethanol. Following drying under reduced pressure at 30 °C, the polymer sample was weighed.

2.7.2. Ethylene polymerization at 10 atm C_2H_4.

The polymerization at 10 atm C_2H_4 was carried out in a stainless steel autoclave (250 mL) which was equipped with an ethylene pressure control system, a temperature controller and a mechanical stirrer. The oven-dried autoclave was placed under vacuum and backfilled with ethylene three times. When the set reaction temperature was reached, the precatalyst (2.0 μmol) dissolved in

freshly distilled toluene (30 mL), was injected into the autoclave. More toluene (30 mL) was then added to wash any residual precatalyst into the autoclave. The required amount of co-catalyst (*i.e.,* MAO, MMAO, EASC, Et_2AlCl) was introduced by syringe followed by more toluene (40 mL) to complete the addition. The autoclave was immediately pressurized to the 10 atm C_2H_4 and the mechanical stirring commenced. After the required reaction time, the ethylene pressure was released and 10% hydrochloric acid in ethanol was used to quench the reaction. The polymer was collected by filtration and washed with ethanol. Following drying under reduced pressure at 30 °C, the polymer sample was weighed.

3. Results and discussion

3.1. Synthesis and characterization of the ligands and complexes

The unsymmetrical 1,2-bis(imino)acenaphthenes, 1-[2,6-{(4-F-C_6H_4)$_2$CH}$_2$-4-{C(CH_3)$_3$}-C_6H_2N]-2-(ArN)$C_2C_{10}H_6$ (Ar = 2,6-$Me_2C_6H_3$ **L1**, 2,6-$Et_2C_6H_3$ **L2**, 2,6-*i*-$Pr_2C_6H_3$ **L3**, 2,4,6-$Me_3C_6H_2$ **L4**, 2,6-Et_2-4-MeC_6H_2 **L5**) have been prepared by a two-step procedure. Firstly, 2-[2,6-bis(bis(4-fluorophenyl)methyl)-4-*t*-butylphenylimino]-acenaphthylen-1-one [38,39], was synthesized in good yield by the acid-catalyzed condensation reaction of acenaphthylene-1,2-dione with one molar equivalent of 2,6-bis(bis(4-fluorophenyl)methyl)-4-*t*-butylaniline. This imine-ketone can then be reacted with the corresponding aniline, 2,6-R^1_2-6-$R^2C_6H_2NH_2$ (R^1 = Me, R^2 = H; R^1 = Et, R^2 = H; R^1 = *i*-Pr, R^2 = H; R^1 = R^2 = Me; R^1 = Et, R^2 = Me) to form, **L1** – **L5**, in moderate to good yield (24 – 37%) (Scheme 1). All the new compounds have been fully characterized by $^1H/^{13}C/^{19}F$ NMR and FT-IR spectroscopy as well as by elemental analysis (see experimental).

Treatment of **L1** – **L5** with either (DME)$NiBr_2$ (DME = 1,2-dimethoxyethane) in dichloromethane or with $NiCl_2·6H_2O$ in a mixture of dichloromethane and ethanol, afforded [1-[2,6-{(4-F-C_6H_4)$_2$CH}$_2$-4-{C(CH_3)$_3$}-C_6H_2N]-2-(ArN)$C_2C_{10}H_6$]$NiBr_2$ (Ar = 2,6-$Me_2C_6H_3$ **Ni1**, 2,6-$Et_2C_6H_3$ **Ni2**, 2,6-*i*-$Pr_2C_6H_3$ **Ni3**, 2,4,6-$Me_3C_6H_2$ **Ni4**, 2,6-Et_2-4-MeC_6H_2 **Ni5**) and [1-[2,6-{(4-F-C_6H_4)$_2$CH}$_2$-4-{C(CH_3)$_3$} -C_6H_2N]-2-ArN)$C_2C_{10}H_6$]$NiCl_2$ (Ar = 2,6-$Me_2C_6H_3$ **Ni6**, 2,6-$Et_2C_6H_3$ **Ni7**, 2,6-*i*-$Pr_2C_6H_3$ **Ni8**, 2,4,6-$Me_3C_6H_2$ **Ni9**, 2,6-Et_2-4-MeC_6H_2 **Ni10**), in

good yield (70 – 87%) (Scheme 1). All nickel complexes have been characterized by elemental analysis as well as by $^{1}H/^{19}F$ NMR and FT-IR spectroscopy. In addition, **Ni3** and **Ni7** have been the subject of single crystal X-ray diffraction studies.

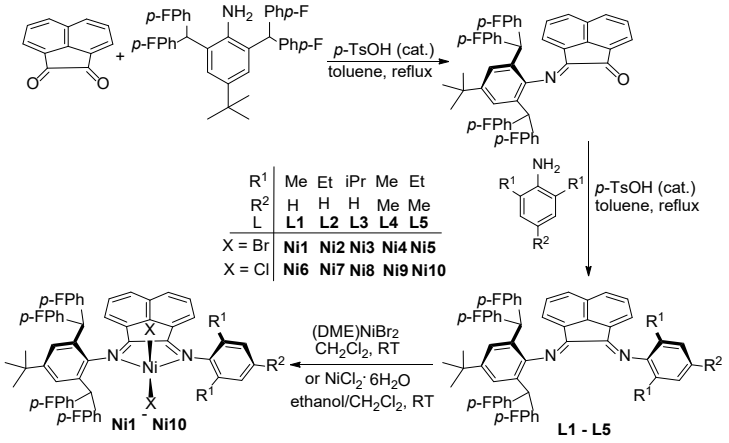

Scheme 1 Synthetic route to **L1 – L5** and their complexes **Ni1 – Ni10**

Single crystals of **Ni3** and **Ni7** of suitable quality for the X-ray determinations were grown by layering diethyl ether onto their dichloromethane solutions at ambient temperature. The molecular structures of **Ni3** and **Ni7** are shown in Figures 1 and 2; selected bond lengths and angles are listed in Table 1. The two structures are closely related and so will be described together. In each case a single nickel center is bound by two halides ligands and two nitrogen donors from the *N,N′*-chelating bis(imino)acenaphthene, to afford a distorted tetrahedral coordination geometry; related α-diimino-nickel(II) halides have been reported elsewhere [27-33]. The key structural difference between **Ni3** and **Ni7** derives from the types of halide ligand [Br (**Ni3**); Cl (**Ni7**)] and the substitution pattern of one of the N-aryl groups (2,6-diisopropyl **Ni3** and 2,6-diethyl **Ni7**). The bite angles of the bidentate ligands [N1-Ni1-N2: 82.68(18)° (**Ni3**), 82.92(16)° (**Ni7**)] are similar, while the X-Ni-X angle shows some variation: Cl1-Ni1-Cl2 122.65(3)° (**Ni3**) *vs.* Br1-Ni1-Br2 128.77(7)° (**Ni7**). The different steric properties of the two aryl groups linked to the bound N atoms results in some disparity in the corresponding nickel-nitrogen bond lengths, with the N1-Ni1 distances in **Ni3** and **Ni7** [2.018(5) Å (**Ni3**), 2.022(4) Å (**Ni7**)] being shorter than those involving N2-Ni1 [2.032(5) Å (**Ni3**), 2.045(4) Å (**Ni7**)]. The C=N bond lengths for the two complexes fall in the range of 1.284(8) – 1.298(6) Å, which are quite typical for this functional group [32]. The plane of the N-aryl group linked to N2 is nearly perpendicular

with respect to the adjacent acenaphthene plane with dihedral angles of 89.3º for **Ni3** and of 89.59º for **Ni7**. On the other hand, the second N-aryl group (aryl = 2,6-*i*-$Pr_2C_6H_3$ **Ni3**; 2,6-$Et_2C_6H_3$ **Ni7**) shows some variation [93.1° **Ni3**, 83.41° **Ni7**]. There are no intermolecular contacts of note.

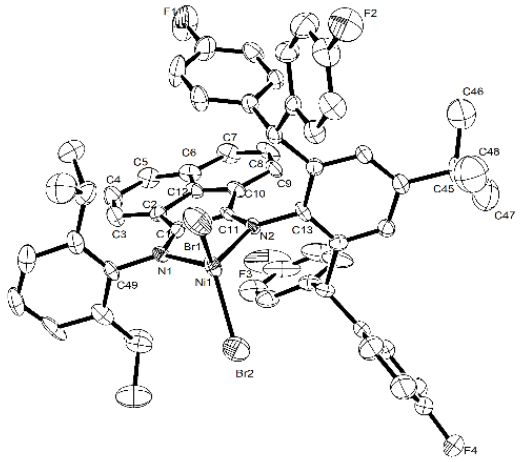

Figure 1 ORTEP representation of **Ni3**. Thermal ellipsoids are shown at the 30% probability level while the hydrogen atoms and two molecules of dichloromethane have been omitted for clarity.

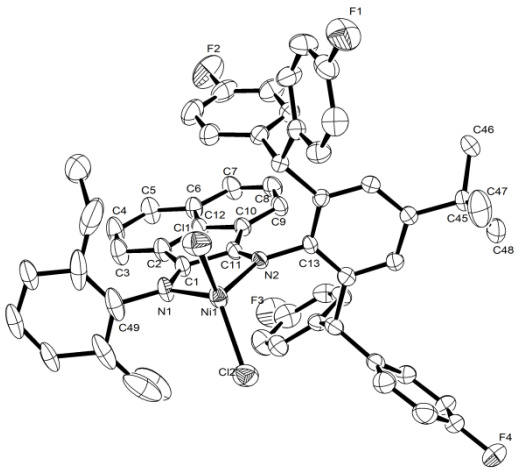

Figure 2 ORTEP representation of **Ni7**. Thermal ellipsoids are shown at the 30% probability level while the hydrogen atoms and a molecule of diethyl ether have been omitted for clarity.

Table 1 Selected bond lengths (Å) and angles (°) for **Ni3** and **Ni7**

	Ni3	**Ni7**
X	Br	Cl
Bond lengths (Å)		
Ni(1)–X(1)	2.3363(10)	2.2062(17)
Ni(1)–X(2)	2.3226(12)	2.1952(17)
Ni(1)–N(1)	2.018(5)	2.022(4)
Ni(1)–N(2)	2.032(5)	2.045(4)

N(1)–C(1)	1.284(8)	1.298(6)
N(1)–C(49)	1.449(7)	1.443(7)
N(2)–C(11)	1.285(8)	1.294(6)
N(2)–C(13)	1.449(7)	1.439(6)
Angles (°)		
X(1)–Ni(1)–X(2)	122.65(3)	128.77(7)
N(1)–Ni(1)–N(2)	82.68(18)	82.92(16)
N(1)–Ni(1)–X(1)	111.65(14)	106.26(16)
N(1)–Ni(1)–X(2)	110.30(13)	111.42(15)
N(2)–Ni(1)–X(1)	110.57(13)	109.38(13)
N(2)–Ni(1)–X(2)	111.94(13)	108.56(14)

All the complexes are paramagnetic as shown by their ^{1}H NMR spectra which show broad shifted peaks in the range δ +35 to -17 (in $CDCl_3$ at ambient temperature) (see Figures 3 and S7). Despite this paramagnetism some peak assignment has been made on the basis of a comparison with data recorded for closely related nickel(II) complexes [32,40]. For example, the acenaphthene protons in each complex can be identified as six independent signals between δ +26 to +5 on account of the asymmetric nature of the ligand backbone, while a broad 2H-peak between δ 11.76 and 13.64 can be assigned to the C*H*(4-FC_6H_4)$_2$ protons. Interestingly, the type of halide bound to the nickel center has an effect on the chemical shifts of otherwise equivalent protons. Taking **Ni3** and **Ni8** as a representative pair, the *para*-aryl proton can be seen upfield at δ -16.22 in **Ni3** while in **Ni8** at δ -14.75 (Figure 3). Similarly, some movement in the resonance for the *t*-butyl protons is evident with the signal seen at δ 3.65 for bromide **Ni3** while in chloride **Ni8** it is shifted slightly downfield to δ 4.47.

We have also investigated the use of ^{19}F NMR spectroscopy to characterize **Ni1** – **Ni10**. Using **Ni3** and **Ni8** again as the representative examples, the spectra are discussed this time alongside the spectrum for corresponding free ligand **L3** (Figure 3). In **L3** the ^{19}F NMR spectrum shows two closely located signals which is consistent with some restricted C_{ortho}-aryl rotation leading to inequivalent CH(4-FC_6H_4)$_a$(4-FC_6H_4)$_b$ groups. Likewise, two signals are seen for bromide **Ni3** in this case with a greater separation. Unexpectedly, the chloride complex **Ni8** displays three distinct fluoride resonances in a 2:0.65:1.35 ratio

(Figure 3 and S10). It remains uncertain however, as to the origin of these differences between the bromide and chloride complexes.

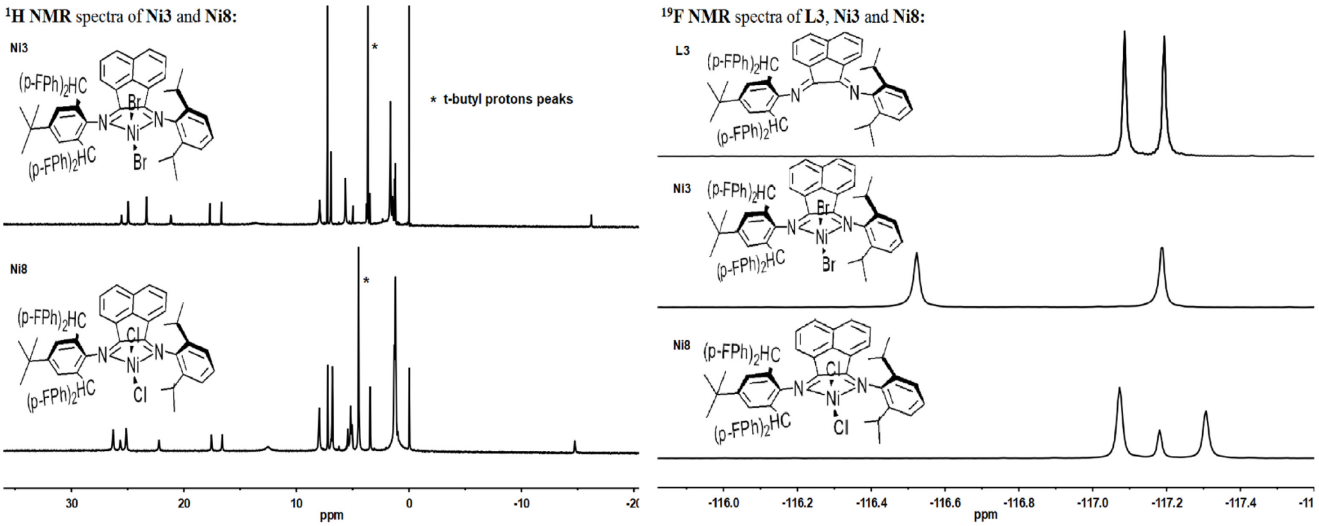

Figure 3 The effect of the halide ligand on the chemical shift of the resonances in the ^{1}H and ^{19}F NMR spectra of **Ni3** and **Ni8**.

In the IR spectra the range in $\nu_{C=N}$ absorptions observed for the free ligands shows some differences when compared to those seen in their complexes. Specifically, in **L1** – **L5** they fall around 1668-1640 cm^{-1} while in **Ni1** – **Ni10** they are shifted to a lower wavenumber range, 1651-1621 cm^{-1}; such shifts are supportive of effective coordination between the nickel ion and the imine-nitrogen atoms [12,13]. In addition, each complex reveals two distinct $\nu_{C=N}$ bands for the two inequivalent types of coordinated imine.

3.2. Co-catalyst screen for ethylene polymerization

In order to identify the most suitable co-catalyst among methylaluminoxane (MAO), modified methylaluminoxane (MMAO), ethylaluminum sesquichloride ($Et_3Al_2Cl_3$, EASC) and diethylaluminum chloride (Et_2AlCl), bromide-containing **Ni5** was selected as the test precatalyst to be investigated. The results are collected in Table 2. The catalytic activities are generally high peaking at 12.7 × 10^6 g PE mol^{-1} (Ni) h^{-1} using EASC and then decrease in the order: EASC > MAO > Et_2AlCl > MMAO [41-44]. In common to all four types of co-catalyst, good activities of more than 8.59 × 10^6 g PE mol^{-1} (Ni) h^{-1} are achieved with molecular weights for the polyethylenes in the 10^5 g mol^{-1} range [56]. However, based on

the numerical values of the catalytic activities, MAO and EASC were chosen for the subsequent more in-depth catalytic evaluations.

Table 2 Ethylene polymerization using **Ni5** with four different co-catalysts[a]

Entry	Co-cat.	Al:Ni	Mass (g)	Activity[b]	M_w	M_w/M_n[c]	T_m[d] (°C)
1	MAO	2500	11.8	11.8	4.41	2.35	69.2
2	MMAO	2500	8.59	8.59	4.76	2.03	49.8
3	Et_2AlCl	400	10.9	10.9	4.73	2.40	78.8
4	EASC	400	12.7	12.7	4.53	2.16	55.9

[a] General conditions: 2.0 μmol of **Ni5**, 100 mL of toluene, 10 atm C_2H_4, 30 min run time, 30 °C run temperature.
[b] $\times 10^6$ g PE mol^{-1} (Ni) h^{-1}.
[c] M_w: $\times 10^5$ g mol^{-1}, determined by GPC.
[d] Determined by DSC.

3.3. Ethylene polymerization using Ni1 – Ni10/MAO

In the first instance, **Ni5**/MAO was screened at 1 atm C_2H_4. To optimize the catalyst, the Al:Ni molar ratio and the run temperature have all been systematically varied; the results of the polymerization tests are compiled in Table 3. With the run time and temperature fixed at 30 minutes and 30 °C, respectively, the highest activity of 9.32×10^5 g PE mol^{-1} (Ni) h^{-1} was observed with an Al:Ni molar ratio of 2750 (entry 5, Table 3). Subsequently, the run temperature was raised from 20 to 60 °C (entries 5 and 7 - 10, Table 3), with the topmost activity of 1.01×10^6 g PE mol^{-1} (Ni) h^{-1} reached at 40 °C (entry 8, Table 3). However, a steady drop in molecular weight of the polyethylene was observed across the entire temperature range ($2.75 - 1.34 \times 10^5$ g mol^{-1}) which can be attributed to a higher rate of chain termination at higher temperatures. Similarly, the melting temperatures of the polymers (T_m = 46.9 – 12.3 °C) gradually decreased with a rise in the temperature; indeed, the appearance of the polymeric materials obtained at 60 °C was close to liquid-like. These observations are consistent with increased branching leading to reduced crystallinity as the temperature is raised [45,46].

Table 3. Optimization of the polymerization conditions using **Ni5**/MAO at 1 atm C_2H_4[a]

Entry	T (°C)	t (min)	Al:Ni	Activity[b]	M_w[c]	M_w/M_n[c]	T_m[d] (°C)

1	30	30	1000	4.48	2.56	1.97	40.3
2	30	30	1500	5.16	3.10	1.66	42.0
3	30	30	2000	6.37	2.29	1.82	36.6
4	30	30	2500	7.96	2.83	1.49	30.5
5	30	30	2750	9.32	2.65	1.83	32.3
6	30	30	3000	7.58	2.52	1.81	31.5
7	20	30	2750	8.35	2.75	1.54	46.9
8	40	30	2750	10.1	2.14	1.73	17.4
9	50	30	2750	9.52	1.70	1.81	13.7
10	60	30	2750	7.20	1.34	1.84	12.3

[a] General conditions: 2.0 μmol of **Ni5**, 100 mL of toluene, 1 atm C_2H_4.
[b] $\times 10^5$ g of PE (mol of Ni)$^{-1}$ h^{-1}.
[c] M_w: $\times 10^5$ g mol^{-1}, determined by GPC.
[d] Determined by DSC, broad transition peak.

The ethylene pressure was then raised to 10 atm C_2H_4 and the catalyst optimization again performed using **Ni5**/MAO; the results are collected in Table 4. With the run time fixed at 30 minutes, the Al:Ni molar ratio was varied from 2250 to 3250 (entries 1 - 5, Table 4) resulting in a maximum activity of 1.20×10^7 g PE mol^{-1} (Ni) h^{-1} (entry 2, Table 4) being observed with an Al:Ni molar ratio of 2500. On increasing the molar ratio above 2500, the observed decrease in activity would suggest that the rate of chain transfer from the active nickel species to aluminum increased [47].

With the Al:Ni ratio for **Ni5**/MAO retained at 2500, the run temperature was elevated from 20 to 90 °C (entries 2 and 6 - 10, Table 4) with the highest activity of 1.18×10^7 g PE mol^{-1} (Ni) h^{-1} (entry 2, Table 4) observed at 30 °C. Increasing the temperature above 30 °C, led the activities to slowly decrease as a result of partial deactivation of the active species [48] and the lower solubility of ethylene in toluene at elevated temperatures; similar trends have been previously reported for related dibenzhydryl-substituted 1,2-bis(imino)acenaphthene-nickel catalysts [27,30]. It is worthy of note that the activity still remained reasonably high even at 90 °C (1.75×10^6 g PE mol^{-1} (Ni) h^{-1}) (entry 12, Table 4). When compared with structurally related N-2,6-dibenzhydryl-4-*t*-butylphenyl-containing **B** (Chart 1) [29], it is evident that the presence of the difluorobenzhydryl groups leads to an improvement in both the catalytic activity and thermal stability. Meanwhile, the molecular weight of the polyethylene gradually decreased from 10.9 to 1.77×10^5 g mol^{-1} as the

reaction temperature was increased from 20 to 90 °C as a result of an increased rate of chain termination induced by higher temperature (Figure 4) [49]. Closer examination reveals the molecular weight obtained at 20 °C (entry 2, Table 4), dropped sharply as the temperature was raised to 30 °C (entries 2 and 6, Table 4). However at 30 or 40 °C, little difference in molecular weight or catalytic activity was observed which suggested that the highest optimum temperature could been seen at 40 °C, further highlighting the thermal stability of this catalytic system. In terms of the T_m values of the polymers, these were found to gradually fall on increasing the reaction temperature which can be accredited to an increase in branching leading to a reduction in crystallinity of the polyethylene chains. Notably, when the polymerization was performed at 70 or 90 °C, the polymer was almost amorphous and gave no recordable T_m values [45,46].

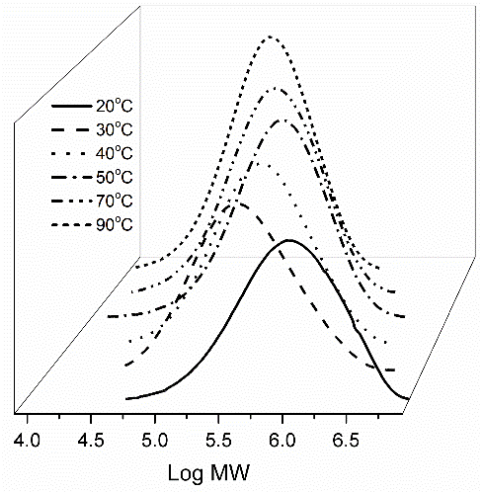

Figure 4 GPC curves of the polyethylenes obtained using **Ni5**/MAO at 10 atm C_2H_4 at various run temperatures (entries 2 and 6 - 10 in Table 4).

With the run temperature kept at 30 °C, the catalytic lifetime of **Ni5**/MAO was probed by recording the activity at different run times, namely 5, 15, 30, 45 and 60 minutes (entries 2 and 11 - 14, Table 4). The best activity of 1.51×10^7 g PE mol^{-1} (Ni) h^{-1} was observed within 5 minutes (entry 11, Table 4). Subsequently, the value steadily decreased with time which suggests that the active species was quickly formed on addition of co-catalyst, then gradually underwent deactivation [24]. Nonetheless, the activity still maintained a

remarkably high level even after one hour [7.14 × 10^6 g PE mol^{-1} (Ni) h^{-1}], highlighting the appreciable lifetime of this catalyst.

With the optimal polymerization conditions established (*viz*., Al:Ni molar ratio of 2500, run temperature of 30 °C, run time of 30 minutes and 10 atm C_2H_4), the remaining nine precatalysts were also evaluated and their results compared alongside **Ni5** (entries 15 - 23, Table 4). All the bromide complexes (**Ni1** – **Ni5**) (entries 2, 15 - 23, Table 4) displayed excellent activities and afforded high molecular weight polyethylene. In terms of their relative performance, their catalytic activities were found to fall in the order, **Ni1** [2,6-di(Me)] > **Ni2** [2,6-di(Et)] > **Ni4** [2,4,6-tri(Me)] > **Ni5** [2,6-di(Et)-4-Me] > **Ni3** [2,6-di(*i*-Pr)], highlighting the combined influence of steric and electronic factors. In particular, the least bulky **Ni1** showed the highest catalytic activity of 12.4 × 10^6 g PE mol^{-1} (Ni) h^{-1} (entry 15, Table 4), while the most bulky **Ni3** the least; related performance characteristics have been reported elsewhere [27-33,50-55]. In addition, the polyethylene obtained using **Ni3** [2,6-di(*i*-Pr)] exhibited the highest molecular weight (7.17 × 10^5 g mol^{-1}, entry 17, Table 4) of the **Ni1** – **Ni5** series, underlining the ability of the more bulky substituents to protect the active species and inhibit chain termination reactions. On the other hand, this system generated polymer with the lowest T_m's indicative of the material displaying the lowest crystallinity and highest degree of branching.

Table 4 Ethylene polymerization using **Ni1** – **Ni10** /MAO at 10 atm C_2H_4[a]

Entry	Precat.	T (°C)	t (min)	Al:Ni	Activity[b]	M_w[c]	M_w/M_n[c]	T_m[d] (°C)
1	**Ni5**	30	30	2250	9.18	6.21	2.05	47.9
2	**Ni5**	30	30	2500	11.8	4.41	2.35	69.2
3	**Ni5**	30	30	2750	11.1	4.58	2.02	87.7
4	**Ni5**	30	30	3000	8.87	5.05	2.10	51.4
5	**Ni5**	30	30	3250	7.33	4.71	2.14	68.2
6	**Ni5**	20	30	2500	6.26	10.9	2.33	92.4
7	**Ni5**	40	30	2500	9.87	4.20	2.14	44.9
8	**Ni5**	50	30	2500	6.37	3.63	2.08	39.4
9	**Ni5**	70	30	2500	4.57	2.29	2.24	-[e]
10	**Ni5**	90	30	2500	1.75	2.03	1.62	-[e]
11	**Ni5**	30	5	2500	15.1	4.05	1.83	58.1
12	**Ni5**	30	15	2500	11.9	4.42	2.06	64.5

13	**Ni5**	30	45	2500	8.75	4.44	2.11	53.9
14	**Ni5**	30	60	2500	7.14	4.44	2.15	51.7
15	**Ni1**	30	30	2500	12.4	3.32	2.95	56.3
16	**Ni2**	30	30	2500	12.0	4.20	2.09	54.8
17	**Ni3**	30	30	2500	7.81	7.17	2.11	45.4
18	**Ni4**	30	30	2500	11.9	7.04	2.57	54.0
19	**Ni6**	30	30	2500	9.65	3.59	2.26	55.9
20	**Ni7**	30	30	2500	9.57	4.54	2.18	59.5
21	**Ni8**	30	30	2500	8.84	6.40	2.35	52.1
22	**Ni9**	30	30	2500	9.34	5.15	2.14	59.6
23	**Ni10**	30	30	2500	9.33	4.53	1.98	53.9

[a] General conditions: 2.0 μmol of precatalyst, 100 mL of toluene, 10 atm C_2H_4.
[b] $\times 10^6$ g PE mol^{-1} (Ni) h^{-1}.
[c] M_w: $\times 10^5$ g mol^{-1}, determined by GPC.
[d] Determined by DSC.
[e] Broad and weak endotherms, amorphous polymers.

Under identical polymerization conditions, the catalytic activities of the nickel chlorides (**Ni6** – **Ni10**) were generally lower than that seen for bromide-containing **Ni1** – **Ni5**, but nevertheless showed a similar trend: **Ni6** [2,6-di(Me)] > **Ni7** [2,6-di(Et)] > **Ni8** [2,6-di(*i*-Pr)] > **Ni9** [2,4,6-tri(Me)] > **Ni10** [2,6-di(Et)-4-Me]. Indeed, the catalytic activities of all the nickel bromide complexes were generally above 11.8 × 10^6 g PE mol^{-1} (Ni) h^{-1} (except **Ni3**), which compares with around 9.0 × 10^6 g PE mol^{-1} (Ni) h^{-1} for the chlorides. These activity differences between chloride and bromide precatalysts have been noted in other catalytic systems and one possible explanation may be attributed to variations in the counterion generated following activation [27-33]. Once again the more sterically hindered 2,6-diisopropyl **Ni8**, afforded the highest molecular weight polymer of this series [6.40 × 10^5 g mol^{-1}] and gave the lowest T_m. As a general finding for all these MAO-activated systems in this study, a relatively narrow range for their molecular weight distributions was observed (M_w/M_n = 1.98 – 2.35) indicative of single site type behavior of the active species.

3.4. Ethylene polymerization using Ni1 – Ni10/EASC

As with the **Ni5**/MAO study, **Ni5**/EASC was also evaluated as a catalyst under two different pressure regimes; the results of polymerization tests performed at lower pressure will be

discussed first. Under 1 atm C_2H_4, the standout catalytic performance (1.20×10^6 g PE mol^{-1} (Ni) h^{-1}) was shown with an Al:Ni molar ratio of 500 and run temperature of 40 °C. As noted earlier, polymers with higher molecular weights and T_m's were obtained at lower reaction temperatures. All the polymers obtained at temperatures over 40 °C were highly viscous materials which can be credited to the high degree of branching [45,46].

Table 5 Ethylene polymerization using **Ni5**/EASC at 1 atm C_2H_4[a]

Entry	T (°C)	t (min)	Al:Ni	Activity[b]	M_w[c]	M_w/M_n[c]	T_m[d] (°C)
1	30	30	300	5.87	2.48	1.63	41.4
2	30	30	400	7.24	1.94	1.76	30.5
3	30	30	500	11.0	2.09	1.53	34.6
4	30	30	600	9.55	2.90	1.31	34.4
5	30	30	700	9.03	2.28	1.61	42.3
6	20	30	500	8.35	2.77	1.26	52.4
7	40	30	500	12.0	2.01	1.58	31.4
8	50	30	500	10.8	1.71	1.87	22.3
9	60	30	500	8.69	1.11	1.70	17.8

[a] General conditions: 2.0 μmol of **Ni5**, 100 mL of toluene, 1 atm C_2H_4.
[b] $\times 10^5$ g PE mol^{-1} (Ni) h^{-1}.
[c] M_w: $\times 10^5$ g mol^{-1}, determined by GPC.
[d] Determined by DSC, broad transition peaks.

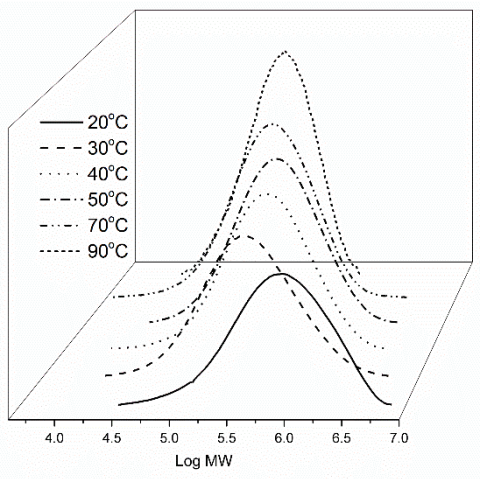

Figure 5 GPC curves for the polyethylenes obtained using **Ni5**/EASC at 10 atm C_2H_4 at various run temperatures (entries 2 and 6 - 10 in Table 6).

With the ethylene pressure now increased to 10 atm, **Ni5**/EASC was again optimized by varying the Al:Ni ratio and run temperature; the results are collected in Table 6. Firstly, the best catalytic performance (1.27×10^7 g PE mol^{-1} (Ni) h^{-1} was achieved with a Al:Ni ratio

value of 400 (entry 2, Table 6). In comparison with **Ni5**/MAO, a slightly higher peak activity [11.8 × 10^6 g PE mol^{-1} (Ni) h^{-1}, entry 2, Table 4] was observed with **Ni5**/EASC which agreed with the results of the lower pressure runs [1.10 × 10^6 g PE mol^{-1} (Ni) h^{-1} (EASC) *vs.* 9.32 × 10^5 g PE mol^{-1} (Ni) h^{-1} (MAO)]. On the other hand, the use of **Ni5**/EASC afforded polymers that showed lower molecular weight and narrower polydispersity [4.53 – 11.7 × 10^5 g mol^{-1}; M_w/M_n = 1.54 – 2.33].

To examine the thermal stability of **Ni5**/EASC, the polymerizations were performed at temperatures between 20 and 90 °C (entries 2, 6 - 10, Table 6) with the highest activity of 1.27 × 10^7 g PE mol^{-1} (Ni) h^{-1} noted at 30 °C. Little variation in catalytic activity was, however, seen with the temperature increased to 40 °C (1.10 × 10^7 g PE mol^{-1} (Ni) h^{-1}). By contrast, above 40 °C there was a steady decline as the temperature was raised reaching its lowest value at 90 °C (4.34 × 10^6 g PE mol^{-1} (Ni) h^{-1}). Nonetheless, this high temperature activity can still be regarded as good and higher than that seen with **Ni5**/MAO at the same temperature (1.75 × 10^6 g PE mol^{-1} (Ni) h^{-1}, entry 10, Table 4). On the other hand, the polymers obtained at higher temperature showed lower T_m values resulting from lower crystallinity and indeed between 70 and 90 °C no reliable DSC measurements could be made, findings that are consistent with the highly branched nature of the polymer [45,46]. As observed before, the highest molecular weight polymers (13.1 × 10^5 g mol^{-1}, entry 6, Table 6) were generated at 20 °C (see Figure 5). On varying the reaction time from 5 to 60 minutes (entries 2, 11 - 14, Table 6), a similar deactivation profile was observed to that seen with **Ni5**/MAO with a peak in activity of 1.84 × 10^7 g PE mol^{-1} (Ni) h^{-1} seen after 5 minutes (*c.f.* 1.51 × 10^7 g PE mol^{-1} (Ni) h^{-1} for **Ni5**/MAO).

Using the optimized conditions established for **Ni5**/EASC (Al:Ni molar ratio = 400, run temperature = 30 °C, run time = 30 minutes, C_2H_4 pressure = 10 atm), the remaining nine catalysts were similarly screened (entries 2, 15 - 23, Table 6). All catalysts exhibited high activity producing polyethylenes of molecular weights falling in the 10^5 g mol^{-1} range. For the nickel bromides, their activities followed the order, **Ni1** [2,6-di(Me)] > **Ni5** [2,6-di(Et)-4-Me] > **Ni2** [2,6-di(Et)] > **Ni4** [2,4,6-tri(Me)] > **Ni3** [2,6-di(*i*-Pr)] (entries 2, 15 - 18, Table 6), which largely mimics the order seen with MAO and further highlights the

importance of steric hindrance and electronic effects on catalytic activity. As a recurring theme, the most sterically hindered **Ni3** showed the lowest activity but the highest molecular weight of this nickel bromide series. Unlike the bromide precatalysts, the activities for the chlorides, **Ni6** – **Ni10**, showed some variation in their relative order: **Ni9** [2,4,6-tri(Me)] > **Ni10** [2,6-di(Et)-4-Me] > **Ni6** [2,6-di(Me)] > **Ni7** [2,6-di(Et)] > **Ni8** [2,6-di(*i*-Pr)]. It is unclear as to the difference but the improved solubility of the *para*-methyl-containing derivatives, **Ni9** and **Ni10**, could be an explanation for these particular systems being the most active. In comparison with **Ni1** – **Ni5** (entries 2, 15 - 18, Table 6), the chloride-containing **Ni6** – **Ni10** (entries 19 - 23, Table 6) generally showed lower activities falling in the range of 8.33 – 12.6 × 10^6 g PE mol^{-1} (Ni) h^{-1}.

Table 6 Ethylene polymerization using **Ni1 - Ni10** /EASC at 10 atm C_2H_4[a]

Entry	Precat.	T (°C)	t (min)	Al:Ni	Activity[b]	M_w[c]	M_w/M_n[c]	T_m[d] (°C)
1	**Ni5**	30	30	300	7.69	8.11	2.12	57.3
2	**Ni5**	30	30	400	12.7	4.53	2.16	55.9
3	**Ni5**	30	30	500	7.84	8.26	2.33	62.8
4	**Ni5**	30	30	600	7.14	11.7	2.14	88.0
5	**Ni5**	30	30	700	3.66	5.79	1.54	60.2
6	**Ni5**	20	30	400	6.90	13.1	2.02	88.3
7	**Ni5**	40	30	400	11.2	4.43	2.19	45.9
8	**Ni5**	50	30	400	6.83	4.33	2.10	44.5
9	**Ni5**	70	30	400	5.29	2.89	2.07	-[e]
10	**Ni5**	90	30	400	4.34	1.88	1.96	-[e]
11	**Ni5**	30	5	400	18.4	7.58	2.03	67.4
12	**Ni5**	30	15	400	13.1	9.91	2.27	74.2
13	**Ni5**	30	45	400	9.15	10.6	2.30	81.6
14	**Ni5**	30	60	400	7.38	7.65	2.52	45.2
15	**Ni1**	30	30	400	13.6	4.23	2.37	54.9
16	**Ni2**	30	30	400	12.1	5.22	2.19	55.9
17	**Ni3**	30	30	400	8.57	6.15	2.33	37.5
18	**Ni4**	30	30	400	11.0	4.23	2.18	54.0
19	**Ni6**	30	30	400	9.50	4.92	2.35	61.6
20	**Ni7**	30	30	400	9.34	5.67	1.71	43.4
21	**Ni8**	30	30	400	8.33	6.04	2.19	42.4
22	**Ni9**	30	30	400	12.6	5.68	2.48	45.9
23	**Ni10**	30	30	400	9.67	4.56	2.10	47.2

[a] General conditions: 2.0 μmol of precatalyst, 100 mL of toluene, 10 atm C_2H_4.

[b] × 10^6 g PE mol^{-1} (Ni) h^{-1}.

[c] M_w: × 10^5 g mol^{-1}, determined by GPC.
[d] Determined by DSC.
[e] Broad and weak endotherms, amorphous polymers.

3.5. Branching properties of the polyethylenes

In general, the T_m's of the polymers generated in this study using either alkyl-aluminum co-catalyst (MAO or EASC), fall in the range 92.4 – 12.3 °C which is in accord with various levels of branching; an observation that is common for nickel polymerization catalysts [27,29] due to their propensity to mediate chain migration/walking [57,58,76-79]. The commonly accepted mechanism is shown in Scheme 2, in which the capacity of the active nickel species to mediate chain isomerization through a sequence of β-H elimination/re-insertion steps is key to the observed branched structures; alternative proposals involving γ- and δ-eliminations have also been proposed [78].

To gain more specific information about the branching and in particular the influence of temperature, co-catalyst and pressure, eight polymer samples were selected for high temperature ^{13}C NMR spectroscopy (recorded in 1,1,2,2-tetrachloroethane-d_2 at 100 °C) (see Figure 6, Figures S1 - S7). In particular, four samples prepared using **Ni5**/MAO at temperatures of 30 °C (PE-$30_{M/1atm}$, PE-$30_{M/10atm}$), 70 °C (PE-$70_{M/10atm}$) and 90 °C (PE-$90_{M/10atm}$) (entry 5, Table 3; entries 2, 9, 10 Table 4) and four samples using **Ni5**/EASC at 30 °C (PE-$30_{E/10atm}$, PE-$30_{E/1atm}$), 70 °C (PE-$70_{E/10atm}$) and 90 °C (PE-$90_{E/10atm}$) (entry 3, Table 5; entries 2, 9, 10, Table 6) were examined. The key findings of the branching analysis are given in Table 7; further details are documented in Tables S1 – S8.

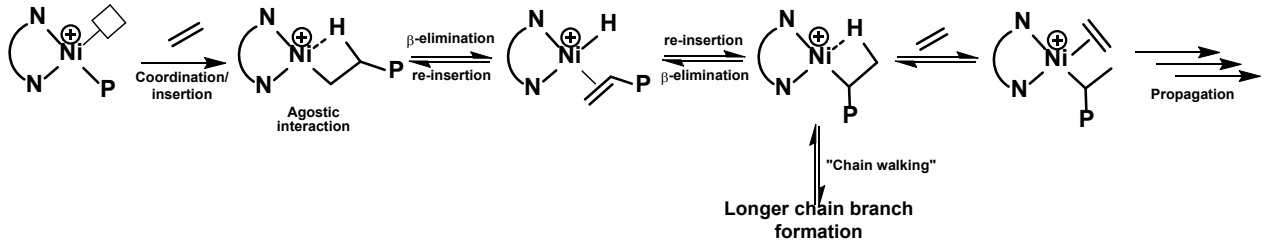

Scheme 2. Chain-walking mechanism commonly accepted for generating branched polyethylenes

Table 7 Branching analysis of the PE samples obtained using **Ni5**/MAO and **Ni5**/EASC at either 10 or 1 atm C_2H_4[a]

	Relative % (N) of Me, Et, Pr, Bu, amyl, 1,4-paired Me, 1,5-paired Me, 1,6-paired Me, longer chains and 1,4-paired longer chains.											
Sample	N_M	N_E	N_P	N_B'	N_A	$N_{M(1,4)}$	$N_{M(1,5)}$	$N_{M(1,6)}$	N_L	$N_{L(1,4)}$	R^b	Branches[c]

PE-$30_{M/10atm}$	56.8	2.0	3.4	6.5	4.7	9.9	0	6.5	6.0	4.3	8.1	157
PE-$70_{M/10atm}$	31.4	6.5	8.2	9.2	6.5	12.9	2.8	10.1	5.1	7.3	5.4	248
PE-$90_{M/10atm}$	22.8	8.0	7.8	11.9	4.2	12.9	5.9	13.9	8.4	4.2	4.3	260
PE-$30_{M/1atm}$	31.0	5.6	5.9	11.7	2.0	12.8	4.6	11.1	13.2	2.1	3.0	231
PE-$30_{E/10atm}$	42.8	2.9	5.9	7.4	7.3	12.6	0	6.8	7.4	7.1	7.3	146
PE-$70_{E/10atm}$	28.1	2.5	4.8	9.9	7.1	17.3	2.3	10.4	8.1	9.5	4.4	222
PE-$90_{E/10atm}$	15.5	7.9	6.6	13.2	3.8	13.7	6.3	15.7	13.8	3.6	3.2	229
PE-$30_{E/1atm}$	27.9	7.3	4.2	11.0	1.5	9.0	7.6	12.9	17.3	1.3	2.6	194

[a] Data determined from their ^{13}C NMR spectra using approaches described elsewhere [59].

[b] Branching R (%) calculated with respect to the total ethylene units $X_{\delta\delta CH2PE}$ present in the polymer: $R\ (\%) = N_M + N_E + N_P + N_B + N_A + N_{M(1,4)} + N_{M(1,5)} + N_{M(1,6)} + N_L + N_{L(1,4)} + X_{\delta\delta CH2PE}$.

[c] Expressed per 1000 C's [73].

On inspection of the results, it is clear that the branching content and branch type are highly influenced by reaction temperature and pressure which in turn links to the relative rates of chain isomerization shown in Scheme 2. With regard to the polymers obtained using **Ni5**/MAO, sample PE-$30_{M/10atm}$ possessed 157 branches per 1000 C's which included most types of branches with the exception of 1,5-paired methyls (Figure 6). It is worthy of note that more than half were short chain with the majority being methyl branches (77.2%). By contrast, PE-$70_{M/10atm}$ and PE-$90_{M/10atm}$, obtained at higher temperatures, gave 248 and 260 branches per 1000 C's, respectively, including some levels of all the branch types listed. On the other hand, relatively few methyl chains (57.2, 55.5%) were present when compared with the sample obtained at 30 °C which highlights the formation of longer and more complicated branching architectures at higher temperatures (Figure S5) [60]. The lower pressure sample, PE-$30_{M/1atm}$, however, gave 231 branches per 1000 C's which is higher than that seen for PE-$30_{M/10atm}$ at higher pressure (see Figure S7), which is consistent with the trend in T_m values [69.2 °C (10 atm) *vs.* 32.3 °C (1 atm)] [31,60]; this branching/ethylene pressure correlation is similar to that observed in our previous findings [31]. In terms of branching type, this lower pressure sample gives the largest proportion of longer chain branches (15.3%) and fewest methyl chains (48.4%); a finding that can be attributed to a decreased rate of trapping and insertion relative to the rate of chain isomerization which is independent of C_2H_4 [60]. It is noteworthy that the levels of branching for PE-$90_{M/10atm}$, PE-$70_{M/10atm}$ and PE-$30_{M/1atm}$ exceed those reported for polyethylenes obtained using structurally related nickel precatalysts [49].

Compared with **Ni5**/MAO, the polymers produced using **Ni5**/EASC at different temperatures showed a lower degree of branching at either 30, 70 or 90 °C but displayed similar trends (Tables

S5 – S7). For example, PE-30$_{E/10atm}$ possessed 146 branches per 1000 C's, while at higher temperatures, PE-70$_{E/10atm}$ and PE-90$_{E/10atm}$ contained 222 and 229 branches per 1000 C's, respectively, with all branching types present. However, these samples contained a lower overall content of methyl (58.1, 51.2%) than that at 30 °C (62.2%) which resulted in a greater proportion of other types of branched chains at higher temperature [31]. For PE-30$_{E/1atm}$, obtained at lower pressure, the branching content was up to 194 branches per 1000 C's with once again a greater presence of longer chains (17.3%) and less methyl branches (48.4%) than seen at 10 atm.

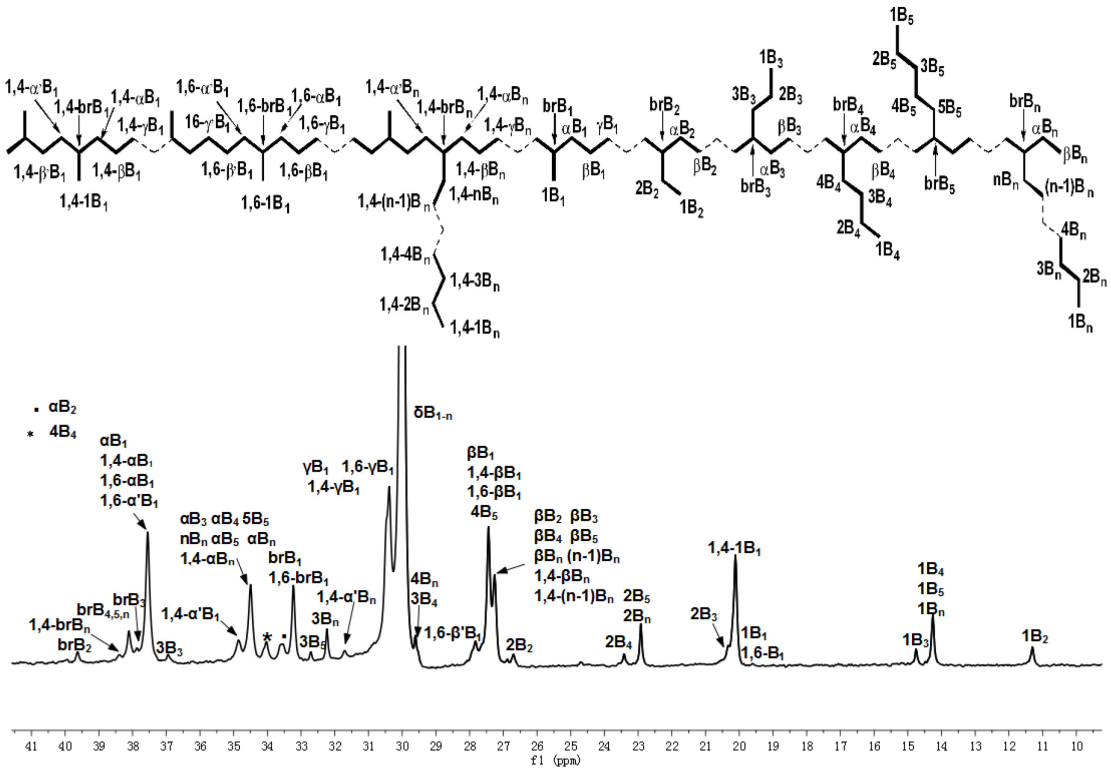

Figure 6 ^{13}C NMR spectrum of PE-30$_{M/10atm}$ obtained using **Ni5**/MAO at 30 °C under 10 atm C_2H_4 (entry 2, Table 4); recorded in tetrachloroethane-d_2 (δC 73.8) at 100 °C (below). Peak assignments are with respect to the depicted polymer backbone (above).

3.6. Mechanical properties of the polyethylenes

With the intent to explore the mechanical properties of these branched materials, eight samples namely, PE-20$_{M/10atm}$ (entry 6, Table 4), PE-30$_{M/10atm}$ (entry 2, Table 4), PE-70$_{M/10atm}$ (entry 9, Table 4), PE-30$_{M/1atm}$ (entry 6, Table 3), PE-20$_{E/10atm}$ (entry 6, Table 6), PE-30$_{E/10atm}$ (entry 2, Table 6), PE-70$_{E/10atm}$ (entry 9, Table 4) and PE-30$_{E/1atm}$ (entry 3, Table 5) obtained using either **Ni5**/MAO or **Ni5**/EASC at 10 atm or 1 atm C_2H_4, were initially selected for assessment. Monotonic tensile stress-strain tests were performed on each sample,

while stress-strain recovery tests using dynamic mechanical analysis (DMA) were conducted solely on the samples prepared using **Ni5**/EASC at 10 atm C_2H_4.

Firstly, the monotonic tensile stress-strain tests were recorded at 20 °C on all eight polymer samples; the data is presented in Table 8 while stress-strain curves are illustrated in Figure 7 [63]. Each mechanical test was performed with five specimens in order to achieve concordant results. For the samples derived from MAO activation and 10 atm C_2H_4, the lowest ultimate tensile stress (2.24 MPa) coupled with the highest strain at break (ε_b = 2839.5%) was observed for PE-$70_{M/10atm}$, which can be attributed to the material being the least crystalline as a result of the high branching content of 248 branches per 1000 C's. As the crystallinity improved in PE-$30_{M/10atm}$ (X_c = 7.1%), the ultimate tensile strength was increased to 6.91 MPa, while the elongation at break decreased to 832.2%. For PE-$20_{M/10atm,}$ the tensile strength reached its highest value (9.38 MPa) while the elongation at break the lowest (ε_b = 507.8%). In comparison with previously reported results obtained with **B** at the same pressure (Chart 1) [29], PE-$30_{M/10atm}$ gave improved ultimate tensile stress as well as a higher elongation at break.

Table 8 Selected properties of PE samples obtained using **Ni5** at various temperatures and C_2H_4 pressures

Sample	T (°C)	T_m (°C)[a]	M_w[b]	Branches /1000 C's	X_c (%)[a]	Stress (MPa)[d]	Strain (%)[d]
PE-$20_{M/10atm}$	20	92.4	10.9	125[c]	9.4	9.38	507.8
PE-$30_{M/10atm}$	30	69.2	4.41	157	7.1	6.91	832.2
PE-$70_{M/10atm}$	70	-[e]	2.29	248	-[e]	2.24	2839.5
PE-$30_{M/1atm}$	30	32.3	1.83	231	0.10	0.02	86.2
PE-$20_{E/10atm}$	20	88.3	13.1	113[c]	10.3	8.64	459.0
PE-$30_{E/10atm}$	30	55.9	4.53	146	8.5	5.01	792.7
PE-$70_{E/10atm}$	70	-[e]	2.89	222	-[e]	1.03	2659.7
PE-$30_{E/1atm}$	30	34.6	1.53	194	0.12	0.06	134.4

[a] Determined by DSC; $X_c = 100 \times \Delta H_f(T_m)/[\Delta H°_f(T°_m)]$, where $\Delta H°_f(T°_m)$ = 248.3 J g^{-1} [38].
[b] Determined by GPC; M_w is expressed as × 10^5 g mol^{-1}.
[c] Determined by FT-IR spectroscopy [62].
[d] The strain or elongation at break (ε_b) was determined using a universal tester.
[e] Broad and weak endotherms, amorphous polymers.

With regard to the samples derived from EASC activation, a similar tensile stress/strain profile was observed with PE-$70_{E/10atm}$ displaying the highest elasticity at break (ε_b) and the lowest ultimate tensile stress, while for PE-$20_{E/10atm}$ the lowest elasticity at break and the highest ultimate tensile stress. Comparison of the polymers obtained by the two different activators at 10 atm C_2H_4 reveals

generally higher values of ε_b with the MAO derived polymers which is in agreement with an earlier study [29]. Overall, it is apparent that the poor crystallinity, resulting from the high branching content, plays a crucial role in the determining these mechanical properties. In general, the polyethylene displaying the higher branching content and lower crystallinity showed the lowest ultimate tensile strength but higher ε_b [64,66,67].

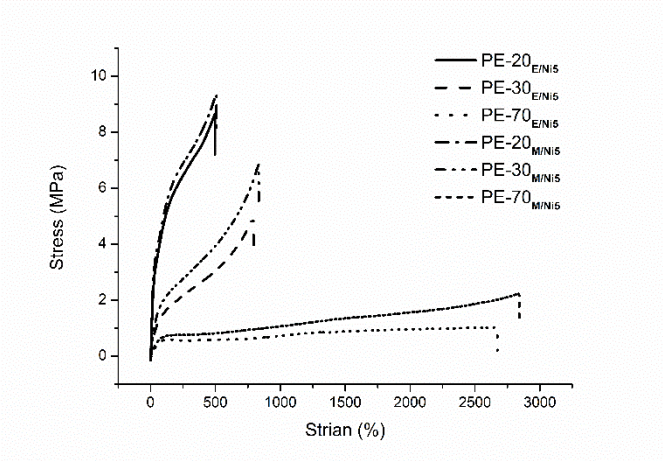

Figure 7 Stress-strain curves for PE-$20_{E/10atm}$, PE-$30_{E/10atm}$, PE-$70_{E/10atm}$, PE-$20_{M/10atm}$, PE-$30_{M/10atm}$ and PE-$70_{M/10atm}$; the vertical line represents the breakage point.

On the other hand, the stress/strain data for the polymers obtained at 1 atm C_2H_4 revealed inferior mechanical properties when compared to those generated at higher pressure [74,75]. For example, by comparing PE-$30_{M/1atm}$ with PE-$70_{M/10atm}$, both the stress (0.02 MPa) and strain (ε_b = 86.2%) for PE-$30_{M/1atm}$ are significantly lower (*c.f.* 2.24 MPa and ε_b = 2839.5% for PE-$70_{M/10atm}$), despite their branching content and molecular weight being comparable (231 *vs.* 248 branches /1000 C's; $M_w = 2.29 \times 10^5$ g mol^{-1} *vs.* 1.83×10^5 g mol^{-1}). Indeed, the weak composition of both lower pressure samples, PE-$30_{M/1atm}$ and PE-$30_{E/1atm}$, made the tests difficult to perform with any reliability. It would seem likely that the higher proportion of longer chain branching has a detrimental effect on the mechanical properties of these materials [68].

Secondly, the stress-strain recovery tests were performed by dynamic mechanical analysis on initially, PE-$20_{E/10atm}$, PE-$30_{E/10atm}$ and PE-$70_{E/10atm}$, to assess their elastomeric properties. However, due to experimental difficulties encountered with PE-$70_{E/10atm}$ (see below), it was substituted with PE-$50_{E/10atm}$. Typically, these tests were performed at -10 and 30 °C and each cycle was repeated up to ten times; the hysteresis curves for PE-$20_{E/10atm}$, PE-$30_{E/10atm}$ and PE-$50_{E/10atm}$ are shown in Figure

8. The observed constant level of recovery after the first cycle is typical for thermoplastic elastomers and can be ascribed to the alignment of the polymer microstructure [67]. As the temperature of the stress-strain recovery tests was increased from -10 to 30 °C, the elastic recovery of PE-$20_{E/10atm}$ was improved from 44 to 46%. Likewise, for PE-$30_{E/10atm}$ and PE-$50_{E/10atm}$, which had similar molecular weights, the elastic recovery increased from 47 to 63% and from 53 to 88%, respectively. Sample PE-$70_{E/10atm}$, which showed the highest ε_b, was also tested with an elastic recovery of 74% when the measurement was performed at -10 °C (Figure S8). However, because of the very high branching content and waxy-like state, the elastic recovery performed at 30 °C could not be satisfactorily measured. As a general finding, it would seem that the elastomeric properties of these polyethylene samples generated at higher pressure were mainly influenced by the crystallinity as opposed to their molecular weight [64,65].

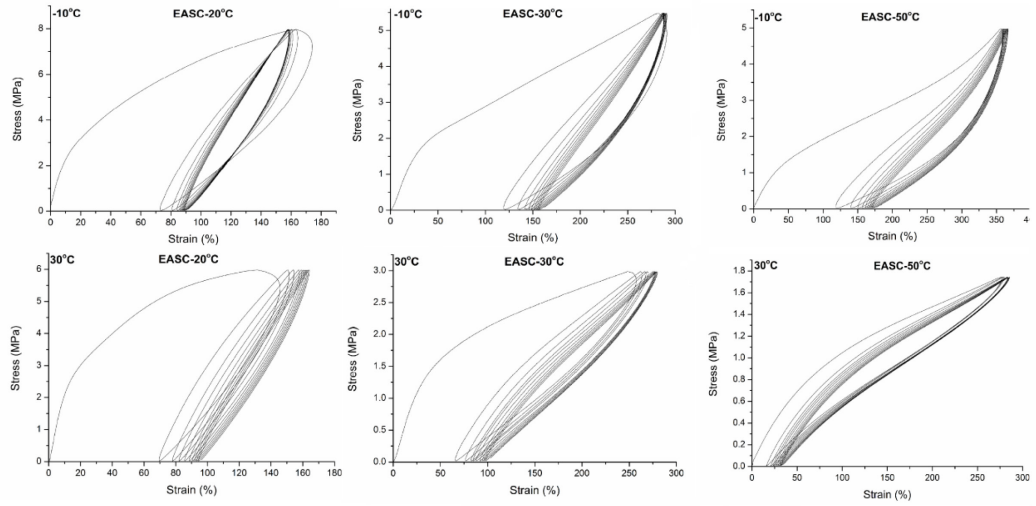

Figure 8 Stress-strain recovery tests for PE-$20_{E/10atm}$, PE-$30_{E/10atm}$ and PE-$50_{E/10atm}$ performed at -10 and 30 °C.

Comparing PE-$30_{M/10atm}$ with a commercial polyolefin elastomer (CPOE) and other thermoplastic elastomers with good mechanical properties reported by our group [29], sample PE-$30_{M/10atm}$ exhibited comparable tensile strength and elastic recovery, properties characteristic of thermoplastic elastomers (TPEs). With regard to the tensile stress, sample PE-$30_{M/10atm}$ exhibited a value of 6.91 MPa which shows a smaller value than CPOE (13.62 MPa) due to the lower X_c value (7.1 *vs.* 14.0%), while their elongation break value is similar (ε_b = 832.2 *vs.* 845%) [69]. In terms of elastic recovery properties, sample PE-$30_{M/10atm}$ displayed lower elastic recovery when compared to

commercial grades (63% *vs.* 85%) [70]. Similarly, this trend was observed when PE-$30_{M/10atm}$ was compared with reported TPEs [29].

4. Conclusions

Ten examples of unsymmetrical 1,2-bis(arylimino)acenaphthene-nickel(II) halide complexes, bearing an N-2,6-diflurobenzhydryl-4-*t*-butyl-phenyl as one of the aryl groups while the other has been varied in terms of its steric and electronic profile, have been successfully prepared and fully characterized by spectroscopic and in two cases by diffraction techniques. On activation with MAO or EASC, all the complexes showed high activities for ethylene polymerization either at 1 or 10 atm C_2H_4 and were capable of maintaining good performance at temperatures up to 90 °C. The narrow molecular weight distributions (M_w/M_n = 1.31 – 1.97 at 1 atm; 1.54 – 2.95 at 10 atm) are supportive of single-site active species. Meanwhile, all the polymers were highly branched and possessed high molecular weights in the order of 10^5 g mol^{-1}. Both pressure and temperature have been shown to affect not only the number of branches but also the degree of short and longer chain branching. Samples displaying moderate crystallinity (X_c = 7 – 10%) at 10 atm C_2H_4 resulted in good elastic recovery properties and in particular samples derived from MAO. By contrast, samples prepared at lower pressure displayed inferior mechanical properties which has been attributed to the higher degree of longer chain branching. Owing to relevance of these materials to TPEs, further investigations are underway to ascertain how we can further control the microstructure of these elastomers using such nickel-mediated ethylene homo-polymerizations.

Supporting Information

^{1}H NMR spectra of Ni1-Ni5, ^{13}C NMR spectra and branching analysis data of the polyethylenes, dynamic mechanical analysis data and X-ray crystallographic studies data. CCDC 1854203 and 1854204 contain the supplementary crystallographic data for this paper. These data can be obtained free of charge via www.ccdc.cam.ac.uk/data_request/cif, or by emailing data_request@ccdc.cam.ac.uk, or by contacting the Cambridge Crystallographic Data Centre, 12 Union Road, Cambridge CB2 1EZ, UK; fax: +44 1223 336033.

Acknowledgements

This work was supported by the National Natural Science Foundation of China (No. 21871275). G.A.S. thanks the Chinese Academy of Sciences for a President's International Fellowship for Visiting Scientists.

References

[1] L. K. Johnson, C. M. Killian, M. Brookhart, J. Am. Chem. Soc. 117 (1995) 6414-6415.

[2] L. K. Johnson, S. Mecking, M. Brookhart, J. Am. Chem. Soc. 118 (1996) 267-268.

[3] D. Meinhard, M. Wegner, G. Kipiani, A. Hearley, P. Reuter, S. Fischer, O. Marti, B. Rieger, J. Am. Chem. Soc. 129 (2007) 9182-9191.

[4] Z. Ye, L. Xu, Z. Dong, P. Xiang, Chem. Commun, 49 (2013) 6235-55.

[5] Z. Guan, Control of Polymer Topology by Chain-Walking Catalysts, Chem. Eur. J. 8 (2002) 3086-3092.

[6] D. H. Camacho, E. V. Salo, J. W. Ziller, Z. Guan, Angew. Chem., Int. Ed. 43 (2004) 1821-1825.

[7] D. H. Camacho, Z. Guan, Chem. Commun. 46 (2010) 7879-7893.

[8] H. Gao, H. Hu, F. Zhu, Q. Wu, Chem. Commun. 48 (2012) 3312-3314.

[9] W. Gao, L. Xin, Z. Hao, G. Li, J. Su, L. Zhou, Y. Mu, Chem. Commun. 51 (2015) 7004-7001.

[10] K. E. Allen, J. Campos, O. Daugulis, M. Brookhart, ACS Catal. 5 (2015) 456-464.

[11] S. A. Svejda, M. Brookhart, Organometallics 18 (1999) 65-74.

[12] H. Liu, W. Zhao, J. Yu, W. Yang, X. Hao, C. Redshaw, L. Chen, W.-H. Sun, Catal. Sci. Technol. 2 (2012) 415-422.

[13] S. Kong, C. Guo, W. Yang, L. Wang, W.-H. Sun, R. Glaser, J. Organomet. Chem. 725 (2013) 37-45.

[14] C. Wen, S. Yuan, Q. Shi, E. Yue, D. Liu, W.-H. Sun, Organometallics 33 (2014) 7223-7231.

[15] X. Wang, L. Fan, Y. Ma, C.-Y. Guo, G. A. Solan, Y. Sun, W.-H. Sun, Polym. Chem. 8 (2017) 2785-2795.

[16] J. L. Rhinehart, N. E. Mitchell, B. K. ACS Catal. 4 (2014) 2501-2504.

[17] W. H. Sun, S. Song, B. Li, C. Redshaw, X. Hao, Y. Li, F. Wang, Dalton Trans. 41 (2012) 11999-2010.

[18] J. Lai, X. Hou, Y. Liu, C. Redshaw, W.-H. Sun, J. Organomet. Chem. 702 (2012) 52-58.

[19] X. Hou, Z. Cai, X. Chen, L. Wang, C. Redshaw, W.-H. Sun, Dalton Trans. 41 (2012) 1617-1623.

[20] X. Hou, T. Liang, W.-H. Sun, C. Redshaw, X. Chen, J. Organomet. Chem. 708 (2012) 98-105.

[21] E. Yue, L. Zhang, Q. Xing, X.-P. Cao, X. Hao, C. Redshaw, W.-H. Sun, Dalton Trans. 43 (2014) 423-431.

[22] E. Yue, Q. Xing, L. Zhang, Q. Shi, X.-P. Cao, L. Wang, C. Redshaw, W.-H. Sun, Dalton Trans. 43 (2014) 3339-3346.

[23] D. Jia, W. Zhang, W. Liu, L. Wang, C. Redshaw, W.-H. Sun, Catal. Sci. Technol. 3 (2013) 2737-2745.

[24] Q. Liu, W. Zhang, D. Jia, X. Hao, C. Redshaw, W.-H. Sun, Applied Catal. A: Gen. 2014) 475, 195-202.

[25] J. Liu, D. Chen, H. Wu, Z. Xiao, H. Gao, F. Zhu, Q. Wu, Macromolecules 47 (2014) 3325-3331.

[26] D. H. Leung, J. W. Ziller, Z. Guan, J. Am. Chem. Soc. 130 (2008) 7538-7539.

[27] H. Liu, W. Zhao, X. Hao, C. Redshaw, W. Huang, W.-H. Sun, Organometallics 30 (2011) 2418-2424.

[28] L. Fan, S. Du, C.-Y. Guo, X. Hao, W.-H. Sun, J. Polym. Sci., Part A: Polym. Chem. 53 (2015) 1369-1378.

[29] Q. Mahmood, Y. Zeng, E. Yue, G. A. Solan, T. Liang, W.-H. Sun, Polym. Chem. 8 (2017) 6416-6430.

[30] S. Du, S. Kong, Q. Shi, J. Mao, C. Guo, J. Yi, T. Liang, W.-H. Sun, Organometallics 34 (2015) 582-590.

[31] X. Wang, L. Fan, Y. Yuan, S. Du, Y. Sun, G. A. Solan, C.-Y. Guo, W.-H. Sun, Dalton Trans. 45 (2016) 18313-18323.

[32] Y. Chen, S. Du, C. Huang, G. A. Solan, X. Hao, W.-H. Sun, J. Polym. Sci., Part A: Polym. Chem. 55 (2017) 1971-1983.

[33] Q. Mahmood, Y. Zeng, X. Wang, Y. Sun, W.-H. Sun, Dalton Trans. 46 (2017) 6934-6947.

[34] D. Guo, L. Han, T. Zhang, W.-H. Sun, T. Li, X. Yang, Macromol, Theory Simul. 11 (2002) 1006-1012.

[35] T. Zhang, D. Guo, S. Jie, W.-H. Sun, T. Li, X. Yang, J. Polym. Sci., Part A: Polym. Chem. 42 (2004) 4765-4774.

[36] T. Zhang, W.-H. Sun, T. Li, X. Yang, J. Mol. Catal. A: Chem. 218 (2004) 119-124.

[37] W. Yang, Y. Chen, W.-H. Sun, Macromol. Chem. and Phy. 215 (2014) 1810-1817.

[38] S. Meiries, K. Speck, D. B. Cordes, A. M. Z. Slawin, S. P. Nolan, Organometallics 32 (2013) 330-339.

[39] J. L. Rhinehart, L. A. Brown, B. K. Long, J. Am. Chem. Soc. 135 (2013) 16316-16319.

[40] B. R. McGarvey, Inorg. Chem. 34 (1995) 6000-6007.

[41] C. G. D. Souza, R. F. D. Souza, K. Bernardo-Gusmão, Applied Catal. A: Gen. 325 (2007) 87-90.

[42] L. C. Simon, R. S. Mauler, R. F. D. Souza, J. Polym. Sci., Part A: Polym. Chem. 37 (1999) 4656-4663.

[43] R. S. Mauler, R. F. D. Souza., D. V. V. Vesccia, L. C. Simon, Macromol. Rapid Commun. 21 (2000) 458-463.

[44] H. Gao, X. Liu, Y. Tang, J. Pan, Q. Wu, Polym. Chem. 2 (2011) 1398-1403.

[45] X. Luo, S. Xie, J. Liu, H. Hu, J. Jiang, W. Huang, H. Gao, D. Zhou, Z. Lü, D. Yan, Polym. Chem. 5 (2014) 1305-1312.

[46] X. Luo, W. Huang, D. Yan, J. Appl. Polym. Sci. 133 (2016) 44127-44135.

[47] G. J. P. Britovsek, S. A. Cohen, V. C. Gibson, M. V. Meurs, J. Am. Chem. Soc. 126 (2004)10701-10712.

[48] C. C. H. Atienza, C. Milsmann, E. Lobkovsky, P. J. Chirik, Angew. Chem., Int. Ed. 50 (2011) 8143-8147.

[49] F. Huang, Z. Sun, S. Du, E. Yue, J. Ba, X. Hu, T. Liang, G. B. Galland, W.-H. Sun, Dalton Trans. 44 (2015) 14281-14292.

[50] B. L. Small, M. Brookhart, A. M. A. Bennett, J. Am. Chem. Soc. 120 (1998) 4049-4050.

[51] G. J. P. Britovsek, V. C. Gibson, S. J. McTavish, G. A. Solan, A. J. P. White, D. J. Williams, G. J. P. Britovsek, B. S. Kimberley, P. J. Maddox, Chem. Commun. (1998) 849-850.

[52] G. J. P. Britovsek, M. Brookhart, V. C. Gibson, B. S. Kimberley, P. J. Maddox, S. Mastroianni, S. J. McTavish, C. Redshaw, G. A. Solan, S. Strömberg, A. J. P. White, D. J. Williams, J. Am. Chem. Soc. 121 (1999) 8728-8740.

[53] A. S. Abu-Surrah, K. Lappalainen, U. Piironen, P. Lehmus, T. Repo, M. Leskel, J. Organomet. Chem. 648 (2002) 55-61.

[54] D. P. Gates, S. A. Svejda, E. Oñate, C.M. Killian, L. K. Johnson, P. S. White, M. Brookhart, Macromolecules 33 (2000) 2320-2334.

[55] Z. Chen, K. E. Allen, P. S. White, O. Daugulis, M. Brookhart, Organometallics 35 (2016) 1756-1760.

[56] S. Du, Q. Xing, Z. Flisak, E. Yue, Y. Sun, W. H. Sun, Dalton Trans. 44 (2015) 12282-12291.

[57] R. Chen, S. F. Mapolie, J. Mol. Catal. A: Chem. 193 (2003) 33-40.

[58] M. M. Wegner, A. K. Ott, B. Rieger, Macromolecules 43 (2010) 3624-3633.

[59] G. B. Galland, R. F. d. Souza, R. S. Mauler, F. F. Nunes, Macromolecules 32 (1999) 1620-1625.

[60] L. Pei, F. Liu, H. Liao, J. Gao, L. Zhong, H. Gao, Q. Wu, ACS Catal. 8 (2018) 1104-1113.

[61] V. Katla, E. Yue, N. M. Rajendran, T. Liang, W.-H. Sun, Comptes Rendus Chimie 19 (2016) 604-613.

[62] T. Usami, S. Takayama, Polym. J. 16 (1984) 731-738.

[63] B. Gabrielle, L. Guy, P.-A. Albouy, L. Vanel, D. R. Long, P. Sotta, Macromolecules 44 (2011) 7006-7015.

[64] Z. He, Y. Liang, W. Yang, H. Uchino, J. Yu, C. Han, W.-H. Sun, Polymer 56 (2015) 119-122.

[65] C. Cobzaru, S. Hild, A. Boger, C. Troll, B. Rieger, Coord. Chem. Rev. 250 (2006) 189-211.

[66] U. Dietrich, M. Hackmann, B. Rieger, M. Klinga, M. Leskela, J. Am. Chem. Soc. 121 (1999) 4348-4355.

[67] B. Rieger, C. Troll, Macromolecules 35 (2002) 5742-5743.

[68] W. Weng, E. J. Markel, A. H. Deknezian, Macromol. Rapid Commun. 22 (2001) 1488-1492.

[69] S. Guo, H. Fan, Z. Bu, B.-G. Li, S. Zhu, Polymer 80 (2015) 109-114.

[70] W. Weng, A. H. Dekmezian, E. J. Markel, D. L. Peters, U.S. Patent, 6184327, (2001).

[71] G. M. Sheldrick, Acta Crystallogr., Sect A: Found. Adv. 71 (2015) 3-8.

[72] G. M. Sheldrick, Acta Crystallogr., Sect C: Struct. Chem. 71 (2015) 3-8.

[73] G. B. Galland, R. Quijada, R. Rojas, G. Bazan, Z. J. A. Komon, Macromolecules 35 (2002) 339-345.

[74] V. Volkis, M. Shmulinson, C. Averbuj, A. Lisovskii, F. T. Edelmann, M. S. Eisen, Organometallics 17 (1998) 3155-3157.

[75] M. Moshonov, S. Aharonovich, M. S. Eisen, Macromolecules 49 (2016) 9287-9290.

[76] Z. Chen, M. Brookhart, Acc. Chem. Res. 51 (2018) 1831-1839.

[77] L. Guo, S. Dai, X. Sui, C. Chen, ACS Catal. 6 (2016) 428-441.

[78] Q. Mahmood, W-H. Sun, R. Soc. Open Sci. 5 (2018) 180367.

[79] D. N. Vaccarello, K. S. O'Connor, P. Iacono, J. M. Rose, A. E. Cherian, G. W. Coates, J. Am. Chem. Soc. 140 (2018) 6208-6211.